

THE GAS CONTENT AND KINEMATICS OF NEARBY BLUE COMPACT GALAXIES: IMPLICATIONS FOR STUDIES AT INTERMEDIATE AND HIGH REDSHIFT

D. J. PISANO AND HENRY A. KOBULNICKY¹

Department of Astronomy, University of Wisconsin, Madison, 475 North Charter Street, Madison, WI 53706; pisano@astro.wisc.edu, chip@astro.wisc.edu

RAFAEL GUZMÁN¹

Department of Astronomy, University of Florida, P.O. Box 112055, Gainesville, FL 32611-2055; rguzman@astro.ufl.edu

JESÚS GALLEGO

Departamento de Astrofísica, Universidad Complutense de Madrid, E-28040 Madrid, Spain; jgm@astrax.fis.ucm.es

AND

MATTHEW A. BERSHADY

Department of Astronomy, University of Wisconsin, Madison, 475 North Charter Street, Madison, WI 53706; mab@astro.wisc.edu

Received 2001 March 20; accepted 2001 June 11

ABSTRACT

We present Arecibo 21 cm spectroscopy, Keck HIRES $H\beta$ spectroscopy, and WIYN R -band imaging of 11 nearby blue compact galaxies with effective B -band surface brightnesses of $S_{\text{Be}} = 19.4\text{--}21.2$ mag arcsec⁻² and effective radii of $R_{\text{eff}} = 0.6\text{--}1.9$ kpc. This sample was selected to test the reliability of mass estimates derived using optical emission line widths, particularly for the blue compact star-forming galaxies observed at intermediate redshifts ($0.1 < z < 1$). In addition, we also measure the H I content and gas depletion timescales for the nearby blue compact galaxies in an attempt to infer the present nature and possible future evolution of their intermediate-redshift analogs. We detected H I in 10 of 11 sample galaxies. They have H I masses of $0.3\text{--}4 \times 10^9 M_{\odot}$, H I line widths, W_{20} , of $133\text{--}249$ km s⁻¹, dynamical masses of 0.5 to $5 \times 10^{10} M_{\odot}$, gas depletion timescales, τ_{gas} , of $0.3\text{--}7$ Gyr, H I mass fractions of $0.01\text{--}0.58$, and mass-to-light ratios of $0.1\text{--}0.8$. These values span the range of values typical of nearby H II galaxies, irregulars, and spirals. Despite the restricted morphological selection, our sample of galaxies is quite heterogeneous in terms of H I content, dynamical mass, and gas depletion timescale. Therefore, these galaxies have a variety of evolutionary paths and should look very different from each other in 5 Gyr. Those with high masses and gas depletion timescales are likely to retain their interstellar medium for future star formation, while the lower mass objects with small gas depletion timescales may be undergoing their last major event of star formation. Hence, the fading of intermediate-redshift, luminous, blue compact galaxies into NGC 205-type spheroidals is a viable evolutionary scenario, but only for the least massive, most gas-poor objects in this sample. The most consistent characteristic of our morphologically selected sample is that the ratios of H II line widths to H I 21 cm line widths, $\mathcal{R} = W_{20}(\text{H II})/W_{20}(\text{H I})$, are systematically less than unity, with an average value of $\mathcal{R} = 0.66 \pm 0.16$, similar to findings for local H II galaxies. The simplest explanation for this result is that the ionized gas is more centrally concentrated than the neutral gas within the gravitational potential. We find that \mathcal{R} is a function of line width, such that smaller line width galaxies have smaller values of \mathcal{R} . Correcting optical line widths by this factor not only raises the derived masses of these galaxies, but also makes them consistent with the local luminosity–line width (Tully-Fisher) relation as well. If this ratio applies to intermediate-redshift galaxies, then the masses of intermediate-redshift, blue compact galaxies can be obtained from optical line widths after applying a small correction factor, and the proposed luminosity evolution of the Tully-Fisher relation is much smaller and more gradual than suggested by studies using optical emission line width measurements.

Key words: galaxies: evolution — galaxies: high-redshift — galaxies: kinematics and dynamics

1. INTRODUCTION

The *Hubble Space Telescope* and the new generation of 8 m class telescopes have extended our knowledge of the early universe by identifying galaxies down to magnitudes of $B \sim 28$ and redshifts of $z \geq 3$ (see review by Ellis 1997). A current challenge is to understand the evolutionary connection between distant galaxies and their nearby counterparts. One approach is to compare fundamental galaxy parameters (i.e., sizes, masses, luminosities) of distant samples with better studied, nearby counterparts to help understand the

harder to observe distant objects and establish evolutionary connections to present-day galaxies.

Studies of high-redshift galaxies have revealed a population of compact, luminous galaxies with high star formation rates (SFRs; see, e.g., Steidel et al. 1996a, 1996b; Lowenthal et al. 1997). At intermediate redshifts, apparently similar sources have been called by various names, including “compact narrow emission line galaxies” (CNELG; Koo et al. 1994; 1995; Guzmán et al. 1996, 1998), “blue nucleated galaxies” (BNG; Schade et al. 1995), and faint, compact galaxies (Guzmán et al. 1997; Phillips et al. 1997), depending on what properties are being emphasized and how the samples were selected. It is worth noting that the term “narrow” in the context of CNELG is with respect to QSOs and AGNs; the CNELGs themselves display a range

¹ Hubble Fellow.

of kinematic emission line widths between 30 and 130 km s⁻¹.

Jangren et al. (2001) have compared several of the brighter of the above intermediate-redshift samples. They find that while the sources display a range of photometric properties, most of the galaxies can be isolated quantitatively on the basis of their colors and image structure parameters as a class distinct from normal Hubble types found in bright samples. They define one such class as “luminous blue compact galaxies” (LBCGs). Sources in this class have small sizes, high luminosities (hence high surface brightnesses), and very blue colors. Their image concentration and asymmetry is slightly higher than for nearby irregular galaxies included in bright samples. However, this class of galaxies is not defined by their emission-line kinematic widths.

The nature and evolution of the LBCG class at intermediate redshift are currently major issues under debate. The most comprehensive studies of the LBCG population at intermediate redshift to date are those of Phillips et al. (1997) and Guzmán et al. (1997). They concluded that the LBCG class is populated by a mixture of starburst galaxies. About 60% of galaxies in their sample are classified as “H π -like,” since they are similar to today’s population of luminous, young, star-forming H π galaxies. The remaining \sim 40% are classified as “SB disklike,” since they form a more heterogeneous class of evolved starbursts similar to local starburst spiral and irregular galaxies. This classification is consistent with the results published for other LBCG samples in the literature. For instance, Koo et al. (1994, 1995) and Guzmán et al. (1996, 1998) first established the association between H π galaxies and LBCGs for their sample of CNELGs. Alternatively, Mallén-Ornelas et al. (1999) and Hammer et al. (2000) have concluded that their LBCG samples can be best identified with bright irregulars, late-type spirals, or even more massive spirals with a very young bulge.

Given the diverse nature of the LBCG population, it is most likely that they will not evolve into one homogeneous galaxy class. Rather, different LBCGs may evolve into different galaxy classes. There are two main evolutionary scenarios currently discussed in the literature. Koo et al. (1994) and subsequent authors have suggested that some subset of the most compact H π -type LBCGs at intermediate redshifts may be the progenitors of local low-mass elliptical galaxies (also called spheroidals), such as NGC 205. Their conjecture is based on the similarity of the kinematic widths and sizes of the LBCGs with low-mass ellipticals. Evolutionary models predict that in 4–6 Gyr of passive evolution, the faded luminosities and surface brightnesses of H π -type LBCGs will match local low-mass ellipticals. This evolutionary prediction requires that LBCGs are undergoing their last major burst of star formation at a $z \sim 0.4$. In order to match the low luminosities of low-mass elliptical galaxies, star formation in H π -type LBCGs must be short-lived (timescales of \sim 1 Gyr or less) so that they fade by \sim 2–4 mag in \sim 4–6 Gyr (Guzmán et al. 1998). Since local low-mass ellipticals have little detectable cool gas (Young & Lo 1997; Young 2000), this prediction also requires H π -type LBCGs to lose nearly all their gas by the present day. Alternatively, the evolutionary scenario for SB disklike LBCGs currently being considered is very different. Some authors have suggested that these LBCGs may actually be disks forming from the center outward to become present-

day spirals (Phillips et al. 1997; Hammer et al. 2000). Thus, SB disklike LBCGs would be more massive than inferred from their virial masses, since their small sizes and kinematic emission-line widths would reflect mainly the central starburst region (Phillips et al. 1997; Barton & Van Zee 2001). These objects are also expected to have large reservoirs of gas that may allow for continuing star formation, albeit at a lower rate than the current burst.

Measurements of the 21 cm neutral hydrogen (H I) line width and flux may provide an important new constraint on the evolution of LBCGs. The H I line width is a very good indicator of the rotational velocity of a galaxy, provided the system is not severely distorted or interacting. We can use this rotational velocity to obtain a total enclosed mass of the system, a parameter that will not change dramatically with time (at least over the past few gigayears), unlike the SFR or luminosity. H I measurements typically trace gas out to a larger radius than the optical emission lines and, hence, offer a more robust measurement of the mass. An integrated H I line flux, coupled with an adopted distance, provides a measure of the total neutral hydrogen mass that limits a galaxy’s potential for future star formation. The H I mass and a known SFR help set limits on the timescale for the reservoir of neutral gas to be depleted.

Since neutral hydrogen observations of the intermediate-redshift LBCGs are not yet possible, we must infer their properties from nearby analogs. This is possible provided the nearby sample is representative of the more distant LBCGs. If observations imply that one of our analogs has a small H I line width, a small quantity of neutral gas, and a short gas depletion timescale, then the case is strengthened for its being a low-mass object that will shortly cease star formation and undergo subsequent passive evolution. If, on the other hand, observations imply a large H I line width, a large reservoir of neutral gas, and a long gas depletion timescale, then the analog would appear to be a higher mass galaxy. A long period of passive evolution following the end of the current starburst would seem less likely, and the galaxy may continue having subsequent events of star formation.

Because we wish to consider sources that span a range of luminosities from “dwarf” ($M_B > -18$) to “luminous” ($M_B < -18$), we adopt here the more generic term blue compact galaxy (BCG) to encompass this diverse group of small, blue galaxies regardless of luminosity or kinematics. Throughout this paper, we will use the sample of compact galaxies in the Hubble Deep Field flanking fields (HDF-ff; Guzmán et al. 1997; Phillips et al. 1997), intermediate-redshift CNELGs (Koo et al. 1994, 1995; Guzmán et al. 1996), and the BNGs of Schade et al. (1995) as a benchmark for assessing a population of local compact galaxies. We will refer to these previous samples collectively as the intermediate-redshift BCGs.

Another issue relating to the study of intermediate-redshift galaxies that we will examine concerns the Tully-Fisher (T-F) relation and its evolution. Specifically, studies of the internal kinematics of intermediate-redshift galaxies have led to discrepant results on the evolution of the T-F zero point. For example, Forbes et al. (1996), Rix et al. (1997), Simard & Pritchett (1998), and Mallén-Ornelas et al. (1999) all find between 1 and 2 mag of brightening in the T-F at redshifts of 0.2–0.8. These surveys rely on [O II] or [O III] and H β emission lines as kinematic tracers; all except Simard & Pritchett measure spatially integrated line

widths. In contrast, studies using resolved rotation curves at intermediate redshifts (Vogt et al. 1996, 1997; Bershadly et al. 1999) find much less brightening (0–0.6 mag) over a range of redshift between 0.1 to 1. Many of these studies specifically target blue galaxies, some of which undoubtedly are BCGs by virtue of their strong emission lines and high surface brightness.

One question that has arisen is whether the spatially integrated line widths of optical emission lines used in some studies underestimate the true rotation velocities. Indeed, Forbes et al. (1996) note that in two cases where they have resolved rotation curves, their line widths underestimate the true rotation speed by 2% and 41%, respectively. Complicating the issue is the fact that the different studies select heterogeneously from the distant galaxy population (Bershadly 1997). If different galaxies evolve at different rates, the measured evolution in the T-F zero point may depend on galaxy types sampled, as suggested by Simard & Pritchett (1998). They find tentative evidence that the least massive (slowest rotators) brighten most. While they have measured rotation curves (albeit at limited spatial resolution and low signal-to-noise ratio), the sense of this observation is the same as would result from the systematic underestimate of true line width based on optical measurements. We are in a position here to address the reliability of internal kinematics based on spatially integrated, optical emission line widths, as well as the conclusions drawn from these measurements.

In this paper, we are presenting H I and H II spectroscopy, as well as *R*-band imaging, of 11 nearby BCGs drawn from the Universidad Complutense de Madrid (UCM) emission-line survey (Zamorano et al. 1994). These galaxies were selected to morphologically resemble the BCG population at intermediate redshift. In § 2, we present the sample selection criteria, observing procedure, and reductions. Section 3 contains the analysis of the data. In § 4, we present our sample galaxies. We discuss the implications of our observations for the inherent nature of BCGs in § 5, and we conclude in § 6. We adopt $H_0 = 70 \text{ km s}^{-1} \text{ Mpc}^{-1}$ and $q_0 = 0.05$ throughout this paper.

2. DATA AND OBSERVATIONS

2.1. Sample Selection

Most BCGs at intermediate redshifts ($z \sim 0.4$) that have been discussed in the literature are intrinsically luminous

objects ($M_B < -18 \text{ mag}$) with blue rest-frame colors ($B - V < 0.45$, $B - r < 0.6$) and are compact in the sense that they have high effective *B*-band surface brightnesses² ($S_{\text{Be}} < 21.5 \text{ mag arcsec}^{-2}$). For this study, we chose galaxies that would be nearby analogs to intermediate-redshift BCGs. Sample galaxies were chosen from the UCM emission-line survey of star-forming galaxies (Zamorano et al. 1994, 1996) based on data from the original survey, follow-up optical spectroscopy (Gallego et al. 1996, 1997), and optical photometry (Vitores et al. 1996a, 1996b; Pérez-González et al. 2000). The survey preferentially selects objects with large H α emission-line equivalent widths, $EW > 50 \text{ \AA}$. Four physical parameters were used to identify the nearby counterparts to the objects observed at intermediate redshift: luminosity, color, velocity dispersion (σ) of the optical emission lines, and effective radius. The criteria were chosen to exclude very low luminosity systems and BCDs, in the classical sense ($M_B \geq -17.0$), to include objects with blue color, $B - r \leq 1.0$, and those with small sizes, $R_{\text{eff}} \leq 2.0 \text{ kpc}$, and small velocity dispersions, $\sigma_{\text{H II}} < 80 \text{ km s}^{-1}$. The important constraint is that our sample galaxies have visible properties similar to BCGs at higher redshifts. We further restricted the sample to objects with declinations between -1° and $+38^\circ$, so that they would be observable from Arecibo. From this limited sample, we chose 11 galaxies that tended to have the smallest velocity dispersions. Table 1 lists the targets selected for observation, their positions, and the time on source, along with alternate identifiers and comments.

In Figure 1 we compare the luminosity, color, size, and surface brightness of the 11 UCM sample galaxies (*filled circles*) with intermediate-redshift BCGs from the HDF-ff (*open triangles*; Phillips et al. 1997; Guzmán et al. 1997) and with a sample of BCGs (*open boxes*); including the CNELGs of Koo et al. 1994, 1995 and the BNGs of Schade et al. 1995). The polygons (from Phillips et al. 1997, Fig. 8) illustrate the approximate location of nearby elliptical, spiral, irregular, and spheroidal galaxies. Figure 1 demonstrates that our sample galaxies have similar surface brightnesses, absolute magnitudes, and colors to the intermediate-redshift BCGs from the literature. In addition, our galaxies

² $S_{\text{Be}} = 5 \log [R_{\text{eff}}(\text{kpc})] + M_B + 38.6$. This is the average surface brightness inside the half-light radius, equivalent to the effective radius for an $r^{1/4}$ profile.

TABLE 1
TARGETS

Name	R.A. (B1950)	Decl. (B1950)	Observation Time (min)	Notes
UCM 0014+1829.....	00 14 39.9	18 29 38	18	
UCM 0040+0220.....	00 40 15.6	02 20 24	24	UM 63
UCM 0056+0043.....	00 56 30.2	00 43 53	12	UM 296
UCM 0135+2242.....	01 35 13.6	22 42 04	42	
UCM 0148+2124.....	01 48 18.5	21 23 53	54	
UCM 0159+2354.....	01 59 00.5	23 54 44	54	
UCM 2251+2352.....	22 51 18.9	23 52 14	18	
UCM 2304+1640.....	23 04 26.2	16 40 02	36	
UCM 2325+2318.....	23 25 11.9	23 18 49	24	NGC 7673, merger?
UCM 2329+2512.....	23 29 36.1	25 12 09	12	
UCM 2351+2321.....	23 51 06.8	23 21 16	48	

NOTE.—Units of right ascension are hours, minutes, and seconds, and units of declination are degrees, arcminutes, and arcseconds.

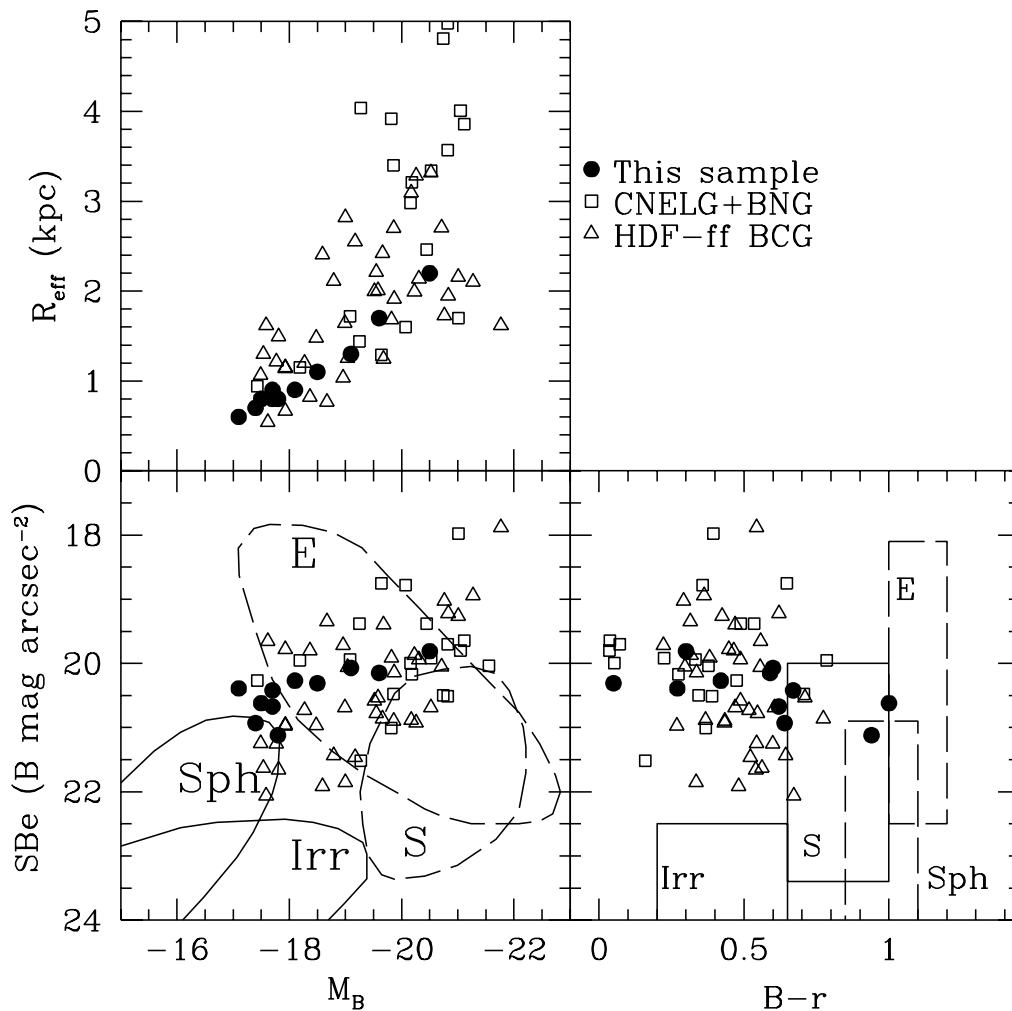


FIG. 1.—Comparison of the selection criteria for 11 UCM sample galaxies (*filled circles*) with CNELGs and BNGs (*squares*) from Jangren et al. (2001) and compact galaxies in the HDF-ff (*triangles*) from Phillips et al. (1997) and Guzmán et al. (1997). The bottom left panel shows absolute magnitude vs. B -band surface brightness and includes polygons outlining the general regions where nearby elliptical (E), spiral (S), irregular (Irr), and spheroidal (Sph) galaxies would lie, based on Guzmán et al. (1997). The bottom right panel shows color $B-r$ vs. B -band surface brightness (SBe), with similar polygons. The top left panel shows the absolute magnitude vs. effective radius, R_{eff} . The sample galaxies have similar luminosities, surface brightnesses, and $B-r$ colors as the more distant BCGs.

have surface brightnesses more similar to low-mass ellipticals and high-mass spheroidals than to massive spirals or irregulars. Some of the targets are on the border between these two classes of objects. While our galaxies do not occupy the full range of parameter space that the intermediate-redshift BCGs do, they are sampling a significant subset of the BCG properties. Our galaxies cover almost the full range of luminosities and colors as the intermediate-redshift BCGs but are only comparable to the smallest of the distant BCGs (with $S_{\text{Be}} \sim 20 \text{ mag arcsec}^{-2}$). These limitations must be remembered when we compare our sample galaxies with their more distant counterparts.

2.2. HI Observations

HI observations of the 11 sample galaxies were made using the Arecibo³ 305 m telescope on 1999 October 14–16. We observed from 2200 to 0400 local sidereal time each day

using the 1.4 GHz feed in conjunction with the L -narrow and L -wide receivers. The L -wide receiver was only used for observations of UCM 0135+2242, while the L -narrow receiver was used for the remaining 10 galaxies. This configuration has a beamwidth of 3.4×3.8 ($79 \times 88 \text{ kpc}$ for a typical galaxy distance of 80 Mpc) and a measured gain of 10 K Jy^{-1} . The system temperature has been measured at 32 K for the L -narrow receiver and 38 K for the L -wide receiver. We observed in four intermediate frequencies (IFs), recording data in two separate bandwidths in both polarizations simultaneously. We observed with bandwidths of 12.5 and 25 MHz with nine-level sampling. This yields a velocity coverage of ~ 2500 and $\sim 5000 \text{ km s}^{-1}$, respectively. With 2048 channels for each IF, the velocity resolution is 1.3 and 2.6 km s^{-1} , respectively. Because the different subcorrelators are not fully independent, we could not combine the two separate bandwidths to improve the sensitivity of our observations.

The observing procedure involved looking at the galaxy for 6 minutes and then doing an off-source scan over the same zenith angle and azimuth range for an additional 6

³ The Arecibo Observatory is part of the National Astronomy and Ionosphere Center, which is operated by Cornell University under a cooperative agreement with the National Science Foundation.

minutes. We repeated observing these on-off pairs until we felt we had a firm detection or that no detection was easily forthcoming. Time on source and measured noise levels for each target are presented in Tables 1 and 2, respectively.

2.3. H I Reductions

Calibration of the data was done using the Arecibo package, ANALYZ. We started by combining each pair of on-off scans by taking the on scans minus the off and then dividing by the off scans. Each combined pair was then corrected for gain and T_{sys} variations with zenith angle and converted from T_b in kelvins to flux in janskys using the tabulated gain factors from the Arecibo users' manual. This factor is roughly 3.6 Jy K^{-1} but varies with the zenith angle of the observation. All scans for a given galaxy were then averaged together. We then averaged the two polarizations for each galaxy together to get a combined unpolarized spectrum. Finally, we did a first- or second-order baseline subtraction on the unpolarized, combined spectrum to get our final, calibrated, reduced spectrum of flux versus heliocentric velocity. As a check on our reductions, we compared the total H I flux with previously published values for UCM 2325 + 2318, otherwise known as NGC 7673. We find that the H I flux agrees to within 5% of the value found by Nordgren et al. (1997a) with the VLA. The data were then ported into IDL for the analysis. Figure 2 shows the calibrated H I spectra for all observed galaxies as light gray lines.

2.4. Keck Echelle Spectroscopy and Reductions

At the Keck I 10 m telescope,⁴ we used the HIRES spectrograph (Vogt et al. 1994) with the blue cross-disperser

⁴ Some of the data presented herein were obtained at the W.M. Keck Observatory, which is operated as a scientific partnership among the California Institute of Technology, the University of California, and the National Aeronautics and Space Administration. The Observatory was made possible by the generous financial support of the W.M. Keck Foundation.

to obtain $R \sim 30,000$ spectra over the wavelength range 3600–5200 Å. Observing occurred on 1999 October 14–15 and 2000 September 14–15. The primary goal was to use the H β $\lambda 4861$ emission line to measure the kinematics of the ionized gas. For two galaxies, UCM 2351 + 2321 and 2325 + 2318, the redshifted H β line fell at the edge of the detector, so we instead used the [O III] $\lambda 4959$ line in the following analysis. The slit decker D1, measuring 1'15 in the spectral direction and 14"0 in the spatial direction, was used for all objects except UCM 0135 + 2242, 0148 + 2123, and 0159 + 2354, for which the C5 slit decker measuring 1'15 \times 7"0 was used. Periodic exposures of a ThAr arc lamp were used to establish the radial velocity and dispersion. The wavelength zero point of each exposure is good to an rms of 0.003 Å. The mean instrumental resolution was 0.12 Å FWHM (7.4 km s^{-1}) at 4900 Å based on exposures of arc lamps. One 1200 s exposure was obtained for each object. During each exposure, the telescope was moved in order to drift the slit slowly across each target to simulate a "spatially integrated" spectrum that would be obtained if all objects were unresolved at large distances. Inspection of the resulting spectra showed that the 14" slit was long enough to cover the entire emission-line region of each galaxy, except in the case of UCM 2325 + 2318, for which portions of the low surface brightness disk extended beyond the ends of the slit. In the reduction process, each spectrum was summed along the spatial dimension to produce a one-dimensional emission-line spectrum. The resulting optical emission-line spectrum for each galaxy is shown overplotted in black on the H I spectrum in Figure 2. There is good correspondence between the H I and H II systemic velocities, confirming that we have correctly identified objects placed at the center of the Arecibo beam. Here W_{20} has been calculated from the H II line for each galaxy observed, and the results appear in Table 2. A comparison of our spatially integrated spectra with the single position spectra of Gallego et al. (2001) show that our values are larger, on average, by 7%, with an rms deviation of 19%. Therefore, the line widths of our galaxies are statistically the same regardless of whether they are measured at a single position or are spatially integrated.

TABLE 2
LINE MEASUREMENTS

Name	rms (mJy channel ⁻¹)	V_{\odot} (km s ⁻¹)	$W_{20}(\text{H I})$ (km s ⁻¹)	$\int Sdv$ (Jy km s ⁻¹)	$W_{20}(\text{H II})$ (km s ⁻¹)	\mathcal{R}^a
UCM 0014 + 1829.....	1.28	5249 \pm 3	204 \pm 5	1.15 \pm 0.05	117 \pm 5	0.57 \pm 0.02
UCM 0040 + 0220.....	1.04	5432 \pm 3	136 \pm 5	0.18 \pm 0.02	96 \pm 5	0.65 \pm 0.04
UCM 0056 + 0043.....	1.52	5352 \pm 3	133 \pm 5	2.1 \pm 0.1	126 \pm 9	0.94 \pm 0.07
UCM 0135 + 2242.....	1.11	10354 \pm 3	249 \pm 5	0.83 \pm 0.04	225 \pm 15	0.90 \pm 0.06
UCM 0148 + 2124.....	0.64	4890 \pm 10	200 \pm 20	0.32 \pm 0.02	98 \pm 8	0.49 \pm 0.06
UCM 0159 + 2354.....	0.48	4901 \pm 3	192 \pm 5	0.52 \pm 0.01	138 \pm 12	0.71 \pm 0.06
UCM 2251 + 2352.....	1.12	7715 \pm 5	140 \pm 10	0.60 \pm 0.03	79 \pm 9	0.56 \pm 0.07
UCM 2304 + 1640.....	0.79	5162 \pm 3	157 \pm 5	0.99 \pm 0.02	85 \pm 6	0.54 \pm 0.04
UCM 2325 + 2318.....	1.07	3412 \pm 3	164 \pm 5	7.21 \pm 0.06	119 \pm 7 ^b	0.72 \pm 0.04
UCM 2329 + 2512.....	1.24	3718 \pm 3	203 \pm 5	2.50 \pm 0.07	88 \pm 6	0.43 \pm 0.03
UCM 2351 + 2321.....	0.68	7943 \pm 3 ^c	...	<0.042 ^d	165 \pm 15	...

^a $\mathcal{R} = W_{20}(\text{H II})/W_{20}(\text{H I})$.

^b An independent measurement by N. Homeier (2000, private communication) using WIYN DensePak H α observations with a 30" \times 45" integral field yields 126 km s⁻¹.

^c Optical velocity from emission lines.

^d 3 σ upper limit over 63 channels (165 km s⁻¹).

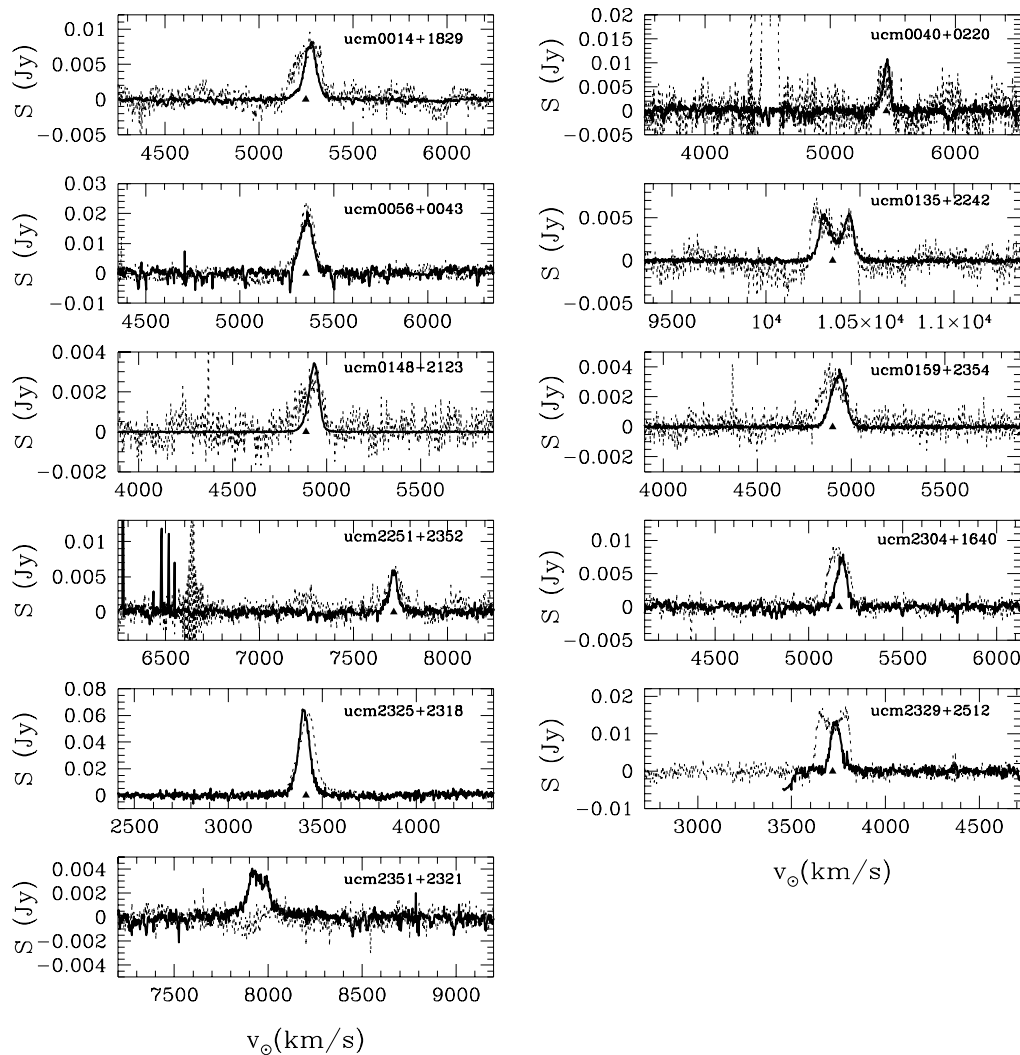


FIG. 2.—H I 21 cm spectra of the sample galaxies plotted as janskys vs. heliocentric recession velocity defined in the optical sense. All but one galaxy is detected. The dark lines are the optical H II emission-line spectra normalized to match the H I Arecibo data (*dashed lines*). The triangles mark the central velocity of the H I profile. This figure shows good agreement between the systemic velocities and profile shapes in H II and H I, but note that the H II lines are systematically more narrow than the H I.

2.5. WIYN Imaging

We obtained *R*-band images of all 11 galaxies with the WIYN⁵ 3.5 m telescope using the Mini-Mosaic 4k × 4k CCD camera during 2000 October 16–17 and November 17–18 in 1".2 (mean) seeing. The pixel scale was 0".141 pixel⁻¹, and integration times were 1–2 × 300 s. The images were reduced in the standard manner. We use these images below to characterize the morphology of each galaxy and supplement the data available in the literature (see, e.g., Vitores et al. 1997; Gallego et al. 1996). Rotational asymmetries, *A*, were computed following the procedures and method specified in Conselice, Bershadsky, & Jangren (2000b); half-light radii, *R*_{eff}, and concentration indices, *C*, were computed following the procedures specified by Ber-

shady et al. (2000). These values are therefore on the same system as computed for the Frei (1999) local galaxy sample by these authors.

Because the half-light radii were in the range of 1".5–9", there were cases when we needed to apply corrections to the asymmetry values, half-light sizes, and concentration indices to account for the seeing. The corrections are in the sense of increasing the asymmetry and image concentration, while decreasing the half-light radius. The corrections for asymmetry are based on the simulations presented in Figure 19 of Conselice et al. (2000b) and generally resulted in changes less than 15%. However, we note that the simulations included only one source plausibly similar to these sources, NGC 4449. To correct the half-light sizes and concentration indices, we modeled the effects of seeing based on a simulated grid of aberrated, two-dimensional, analytic light distributions (*r*^{1/4}-law and exponential profiles with a range of axial ratios). The corrections to the half-light radii were generally under 15%, and the changes in the concen-

⁵ The WIYN Observatory is a joint facility of the University of Wisconsin, Madison, Indiana University, Yale University, and the National Optical Astronomy Observatories.

tration indices were typically a few tenths in the index. A comparison of our half-light radii and concentration indices with previous determinations show agreement of the means to 1% and 28%, with an rms deviation of 21% and 12%, respectively, to Vitores et al. (1996a, 1996b) and 6% and 1% for the mean, with rms deviation of 21% and 17%, respectively, to Pérez-González et al. (2000), with few outliers. Our adopted WIYN values for R_{eff} , C , and A are listed in Table 3. For all subsequent discussions, we will use these values, as determined from the WIYN images.

3. ANALYSIS

For each galaxy, we measured the total H I flux, the 20% velocity width, and the central velocity of each galaxy, as listed in Table 2. The total H I flux was determined by integrating under the spectrum from where the galaxy first appears from the noise to where it becomes indistinguishable from the noise. The rms was measured from the off-line region and used to determine the error on the integrated flux. For UCM 2351 + 2321, which was not detected, the 3σ upper limit to the flux is set for an assumed H I velocity width equal to the optical width as noted in Table 2. The optical velocity widths come from our Keck observations. Since most of the galaxy spectra rise very slowly out of the noise, we Hanning smoothed the spectra to assist in determining the 20% velocity width W_{20} . Typically, we Hanning smoothed over three or five channels, then we used a program to identify all crossings of the 20% of peak intensity. We selected the most probable velocity width from these options. The cited velocity center is simply the midpoint between the 20% crossings. The errors on these values represent the approximate range of widths (and central velocities) because of the uncertainty in determining the 20% crossing points. For UCM 2351 + 2321, the optical recession velocity is cited and is used to calculate a distance because of the lack of a detection in H I. This distance is listed in Table 3 and is used to calculate distance-dependent quantities, such as H I mass, luminosity, and linear size.

We have also attempted to derive the dynamical masses for these galaxies. To do this, we need a rotation velocity and a radius corresponding to that velocity. We used half of the inclination-corrected W_{20} as a reasonable approximation for the rotation velocity. For the corresponding radius R_{HI} , we scaled up the effective radius R_{eff} , determined from our WIYN images, by a factor of 4.5. This factor is based on the ratio of the R_{eff} to the $R_{24.5}$ found for these galaxies in Vitores et al. (1996a, 1996b), which was 2.4. We rounded this up to 2.5 to get an estimate of $R_{2.5}$ and then multiplied $R_{2.5}$ by 1.8 to get R_{HI} , based on the observed ratio of $R_{2.5}$ to R_{HI} found by Broeils (1992) for nearby gas-rich galaxies. The value of R_{HI} may even be higher, since van Zee, Skillman, & Salzer (1998) find $R_{\text{HI}}/R_{2.5}$ ranging from 2.8–4.9 for a sample of five H II galaxies. Using R_{HI} and V_{rot} , we calculate an estimate for the dynamical mass:

$$M_{\text{dyn}} = V_{\text{rot}}^2 R_{\text{HI}}/G. \quad (1)$$

Table 4 lists these dynamical masses, along with the hydrogen gas mass fraction $f_{\text{gas}} = M_{\text{HI}}/M_{\text{dyn}}$. Tables 3 and 4 also list the optical properties of the sample galaxies, including absolute blue magnitudes, M_B , $B-r$ and $B-V$ colors computed within the 24 mag arcsec $^{-2}$ isophote, the effective surface brightness within the 24 mag arcsec $^{-2}$ isophote, the H α luminosity, and the inclination of these galaxies (from Vitores et al. 1996a, 1996b; Gallego et al. 1996, 1997; Pérez-González et al. 2000).

To assist in examining the evolutionary potential of these galaxies, we calculated the SFRs for these galaxies from the listed reddening-corrected H α luminosities (Gallego et al. 1996) using the expression given in Kennicutt (1983):

$$\text{SFR}(M_{\odot} \text{ yr}^{-1}) = \frac{L_{\text{H}\alpha}}{1.12 \times 10^{41} \text{ ergs s}^{-1}}. \quad (2)$$

Using the SFR and the H I mass of each galaxy, we calculate the gas depletion timescale, $\tau_{\text{gas}} = M_{\text{HI}}/\text{SFR}$ listed in Table 4. These estimates do not account for recycling of

TABLE 3
MORPHOLOGICAL PARAMETERS

Name	Distance (Mpc)	M_B (mag)	$B-r$ (mag)	$B-V$ (mag)	R_{eff} (kpc)	Inc. (deg)	SBe (mag arcsec $^{-2}$)	EW (H α) (Å)	C	A
	(1)	(2)	(3)	(4)	(5)	(6)	(7)	(8)	(9)	(10)
UCM 0014 + 1829	75	-18.5	0.05	0.16	1.7	50	21.2	146	4.08	0.08
UCM 0040 + 0220	78	-17.7	0.67	0.50	0.6	30	19.9	97	3.00	0.09
UCM 0056 + 0043	76	-18.1	0.42	0.37	0.9	60	20.3	61	2.96	0.07
UCM 0135 + 2242	148	-19.6	0.59	0.46	1.4	45	19.7	60	4.00	0.02
UCM 0148 + 2124	70	-17.7	0.47	0.48	1.0	40	20.9	150	2.72	0.13
UCM 0159 + 2354	70	-17.5	1.00	0.83	1.0	60	21.1	74	4.25	0.12
UCM 2251 + 2352	110	-19.1	0.59	0.47	1.4	15	20.2	84	3.43	0.27
UCM 2304 + 1640	74	-17.1	0.27	0.28	0.7	45	20.6	155	3.35	0.12
UCM 2325 + 2318	49	-20.5	0.30	0.30	1.9	45	19.4	101	2.98	0.60
UCM 2329 + 2512	53	-17.4	0.64	0.49	0.6	45	19.9	160	4.15	0.02
UCM 2351 + 2321	113	-17.8	0.94	0.77	0.7	35	20.1	117	4.02	0.03

NOTES.—Col. (1): Using D (Mpc) = Velocity/ H_0 ; $H_0 = 70 \text{ km s}^{-1} \text{ Mpc}^{-1}$. Col. (2): Assumes $H_0 = 70$, $q_0 = 0.05$ from Vitores et al. 1996a, 1996b. Col. (3): Observed $B-r$ color from Vitores et al. 1996a, 1996b; typical uncertainties are 0.12 mag. Col. (4): $B-V$ color derived from the observed $B-r$ color, without correction for reddening, assuming an Irregular galaxy spectral energy distribution and $B-V = 0.56(B-r) + 0.136$, based on Fukugita, Shimasaku, & Ichikawa (1995). Col. (5): Effective radius in kiloparsecs from our WIYN photometry, corrected for the effects of seeing and assuming the above cosmology. Col. (6): Inclination, derived from the eccentricity, $e = 1 - b/a$, as in Aaronson, Huchra, & Mould 1980; i (deg) = $\cos^{-1} (1.042E^2 - 0.042)^{1/2} + 3$, where $E = 1 - e$. Typical uncertainties are 15°. Col. (7): Effective surface brightness computed from SBe = $5 \log [R_{\text{eff}}(\text{kpc})] + M_B + 38.6$. Col. (8): H α equivalent width in angstroms (Gallego et al. 1996). Col. (9): Concentration index from our WIYN photometry. Col. (10): Asymmetry parameter from our WIYN photometry.

TABLE 4
DERIVED PARAMETERS

Name (1)	$M_{\text{H I}}$ ($10^9 M_{\odot}$) (2)	$L_{\text{H}\alpha}$ (10^{41} ergs s^{-1}) (3)	SFR ($M_{\odot} \text{ yr}^{-1}$) (4)	τ_{gas} (Gyr) (5)	V_{rot} (km s^{-1}) (6)	$R_{\text{H I}}$ (kpc) (7)	M_{dyn} ($10^{10} M_{\odot}$) (8)	f_{gas} (9)	M/L (M_{\odot}/L_{\odot}) (10)
UCM 0014+1829.....	1.52 ± 0.07	1.09	0.98	1.56	133	7.5	2.9	0.05	0.62
UCM 0040+0220.....	0.26 ± 0.03	0.70	0.63	0.41	146	2.9	1.4	0.02	0.20
UCM 0056+0043.....	2.90 ± 0.11	0.51	0.46	6.34	77	4.1	0.5	0.54	0.20
UCM 0135+2242.....	4.32 ± 0.21	1.87	1.68	2.54	177	6.3	4.4	0.10	0.27
UCM 0148+2124.....	0.38 ± 0.02	0.72	0.65	0.59	155	4.5	2.4	0.02	0.71
UCM 0159+2354.....	0.60 ± 0.01	0.53	0.47	1.27	110	4.5	1.2	0.05	0.78
UCM 2251+2352.....	1.78 ± 0.09	1.89	1.70	1.05	270	6.2	10.0	0.02	0.14
UCM 2304+1640.....	1.28 ± 0.03	0.39	0.35	3.65	110	2.9	0.8	0.16	0.53
UCM 2325+2318.....	4.09 ± 0.03	26.3	23.5	0.18	116	8.3	2.5	0.16	0.07
UCM 2329+2512.....	1.66 ± 0.05	0.25	0.23	7.29	144	2.5	1.2	0.14	0.60
UCM 2351+2321.....	<0.13	1.33	4.53	<0.03	144 ^a	3.2	1.5	≤ 0.01	0.31

NOTES.—Col. (2): H I mass, $M(\text{H I}) = 2.356 \times 10^5 D^2 \int S dv (M_{\odot})$. Col. (3): H α luminosity from Gallego et al. 1996 rescaled to $H_0 = 70$. Col. (4): Star formation rate, $\text{SFR} = L_{\text{H}\alpha}/1.12 \times 10^{41}$, from Kennicutt 1983. Col. (5): Gas depletion timescale, $\tau_{\text{gas}} = M_{\text{H I}}/\text{SFR}$, from Kennicutt 1983. Col. (6): H I rotation velocity corrected for inclination, $V_{\text{rot}} = 0.5 W_{20}/\sin i$. Col. (7): H I radius, $R_{\text{H I}} \sim 4.5 R_{\text{eff}}$; see text for derivation. Col. (8): Dynamical mass corrected for inclination, $M_{\text{dyn}} = V_{\text{rot}}^2 R_{\text{H I}}/G$. Col. (9): $f_{\text{gas}} = M_{\text{H I}}/M_{\text{dyn}}$; mass of molecular gas and ionized gas not included. Col. (10): Mass-to-light ratio at R_{eff} . Mass is calculated from the velocity dispersion, $\sigma = W_{20}(\text{H I})/3.62$, without correcting for inclination. Light is the blue luminosity contained within R_{eff} (i.e., half the total luminosity).

^a From the H II width in Table 2.

the gas, for the presence of helium ($\sim 40\%$ of the H I mass), or for molecular gas. All these factors would increase τ_{gas} .⁶ It is important to note that the $L_{\text{H}\alpha}$ values from Gallego et al. (1996) were measured through the spectrograph slit. Therefore, they only represent a fraction of the total $L_{\text{H}\alpha}$ of the galaxy as would be measured via narrowband imaging. Correcting for this underestimate would decrease our estimates of τ_{gas} . It is unclear, however, how to determine the extent of this correction with our current data.

Images of the target galaxies appear in Figure 3 and 4. Figure 3 shows Digital Sky Survey (DSS) images centered on the observed target coordinates. Each image is 3/8 on a side to match the angular size of Arecibo beam and to assist in determining the nature of the objects we observed. Figure 4 shows the WIYN R-band images of our sample galaxies using a logarithmic gray scale. In order to facilitate comparison between galaxies, we have scaled these images so that each dimension covers a projected distance of 10 kpc at the adopted distances listed in Table 3.

4. GALAXY PROPERTIES

4.1. UCM 0014+1829

Optically, UCM 0014+1829 has an oblong central region with a more diffuse outer disk. There is a bright star very close to the nucleus that complicates the determination of its optical properties. No other galaxies are evident in the DSS image. UCM 0014+1829 has the second largest half-light radius, 1.7 kpc, in our sample and is one of the more concentrated objects as well, $C = 4.08$. It is relatively symmetric, $A = 0.08$. The H I profile is singly peaked and slightly asymmetric. The H II spectrum is symmetric and is centered at the same velocity as the peak of the H I profile, but it is narrower, with a width of 117 versus 204 km s^{-1} . A low amplitude wing to the low velocity is evident in both spectra.

⁶ If we use the updated expression from Kennicutt et al. (1994), the SFR will be lower by $\sim 10\%$ (τ_{gas} will be higher by the same amount). The expression from Alonso-Herrero et al. (1996) will decrease the SFR and increase τ_{gas} by a factor of 2.8.

4.2. UCM 0040+0220

UCM 0040+0220 is the featureless point source in the middle of the DSS image. It has a small size ($R_{\text{eff}} = 0.6$ kpc), is symmetric ($A = 0.09$), and is not very concentrated ($C = 3.0$). This galaxy has one of the smallest τ_{gas} values, 0.41 Gyr, of our sample due, in part, to its low $M_{\text{H I}}$, $2.6 \times 10^8 M_{\odot}$. While there is a strong, double-horned H I profile at $\sim 4500 \text{ km s}^{-1}$, UCM 0040+0220 is the weaker feature at $\sim 5400 \text{ km s}^{-1}$. The other features at higher recession velocities may be real, but we do not have the signal-to-noise ratio in this observation to confirm them. The H I profile is somewhat asymmetric but is hard to characterize because of its low signal-to-noise ratio. The H II spectrum has a tail to lower velocity, similar to that in the H I profile. The double-horned H I profile at $\sim 4500 \text{ km s}^{-1}$ is most likely the diffuse galaxy east of UCM 0040+0220 in the DSS image.

4.3. UCM 0056+0043

Our WIYN image of UCM 0056+0043 reveals that it is slightly extended in the east-west direction. No other galaxies are evident in the DSS image of the field. This galaxy has a half-light radius of 0.9 kpc, an average concentration of 2.96, and a low asymmetry of 0.07. The H I spectrum of UCM 0056+0043 is a strong single peak with weak high velocity wings extending to lower redshift. The profile is slightly asymmetric. The H II spectrum matches the H I profile very closely, with an absence of high-velocity wings. The H II width (126 km s^{-1}) is nearly identical to the H I width (133 km s^{-1}). This galaxy has the smallest width of all our sample galaxies, the smallest dynamical mass ($5 \times 10^9 M_{\odot}$), and the highest gas mass fraction at 0.58. It also has one of the longest gas depletion timescales, 6.3 Gyr.

4.4. UCM 0135+2242

This galaxy has a rather extended, diffuse disk evident in its WIYN image with a large $R_{\text{eff}} = 1.4$ kpc. The concentration is high at 4.0, and the galaxy is very symmetric, $A = 0.02$. UCM 0135+2242 is one of the most massive galaxies in our sample, $M_{\text{dyn}} = 4.4 \times 10^{10} M_{\odot}$, and has a

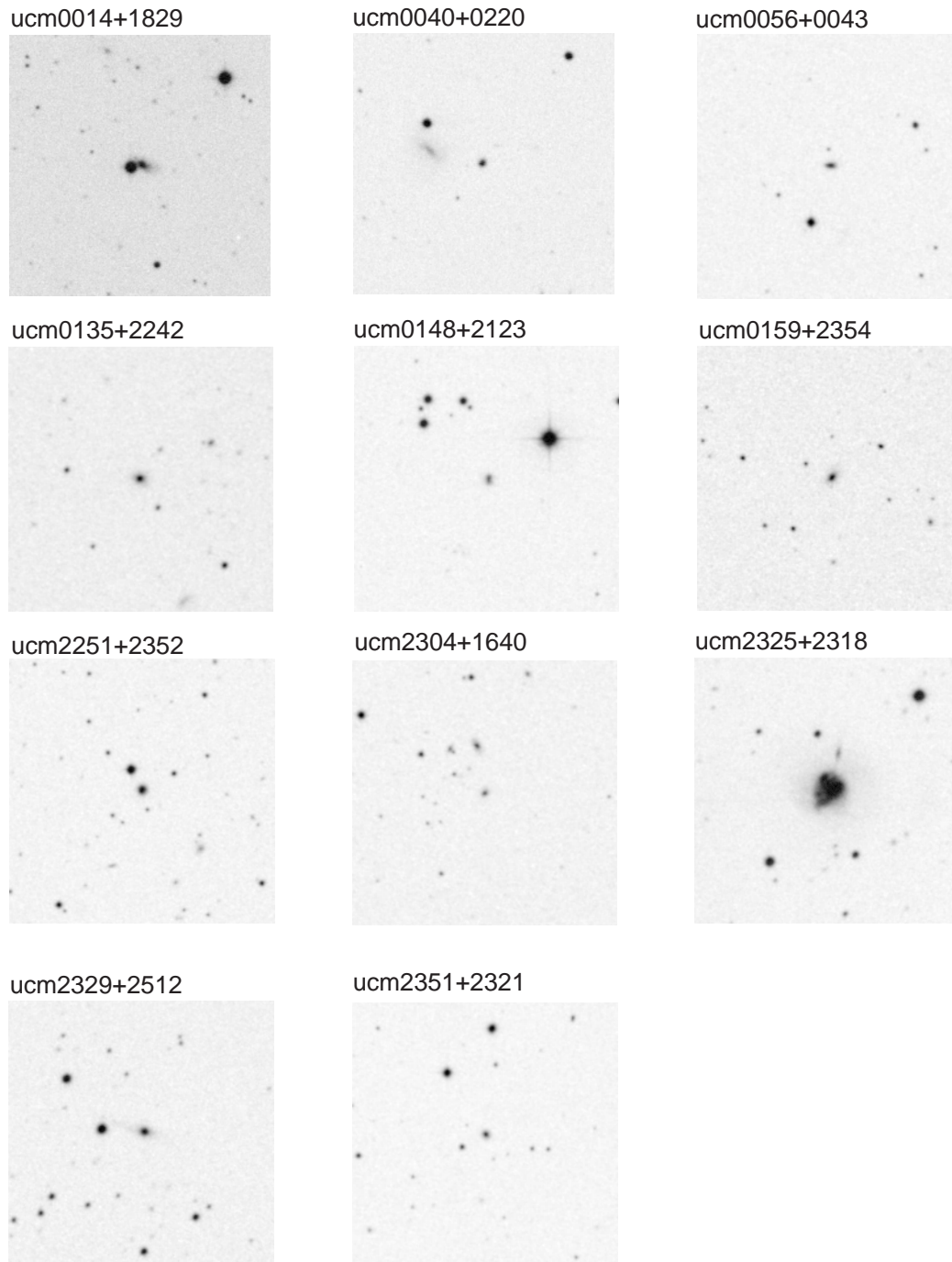


FIG. 3.—Optical images from the DSS, centered on the coordinates observed for each galaxy, showing a patch of sky $3/8$ on a side to match the largest dimension of the Arecibo beam at 21 cm.

long τ_{gas} of 2.5 Gyr, despite its high SFR of $1.7 M_{\odot} \text{ yr}^{-1}$. A potential small companion is evident just to the southwest in the image as well. The DSS image reveals another diffuse galaxy at the southern most extent of the Arecibo field that may or may not be associated. UCM 0135+2242 has a double-horned H I profile that is slightly asymmetric. The H II profile is narrower ($W_{20} = 225 \text{ km s}^{-1}$) and more symmetric than the H I profile ($W_{20} = 249 \text{ km s}^{-1}$). Intriguingly, the low-redshift peak of the H I profile is broader and stronger than the H II peak. In other words, the peak of the H I distribution does not contain corresponding H II emission. This asymmetry in the H I profile and discrepancy

with the H II profile may indicate that multiple galaxies were observed in the Arecibo beam and/or that an interaction has occurred.

4.5. UCM 0148+2123

UCM 0148+2123 either has a double nucleus or is composed of two related objects that are possibly merging based on our WIYN image of the galaxy. No other galaxies are evident in the Arecibo beam. The morphological parameters suggest that this galaxy is not particularly large, $R_{\text{eff}} = 1.0 \text{ kpc}$, nor concentrated, $C = 2.72$, but it is quite asymmetric, $A = 0.13$. The latter point is not surprising given the

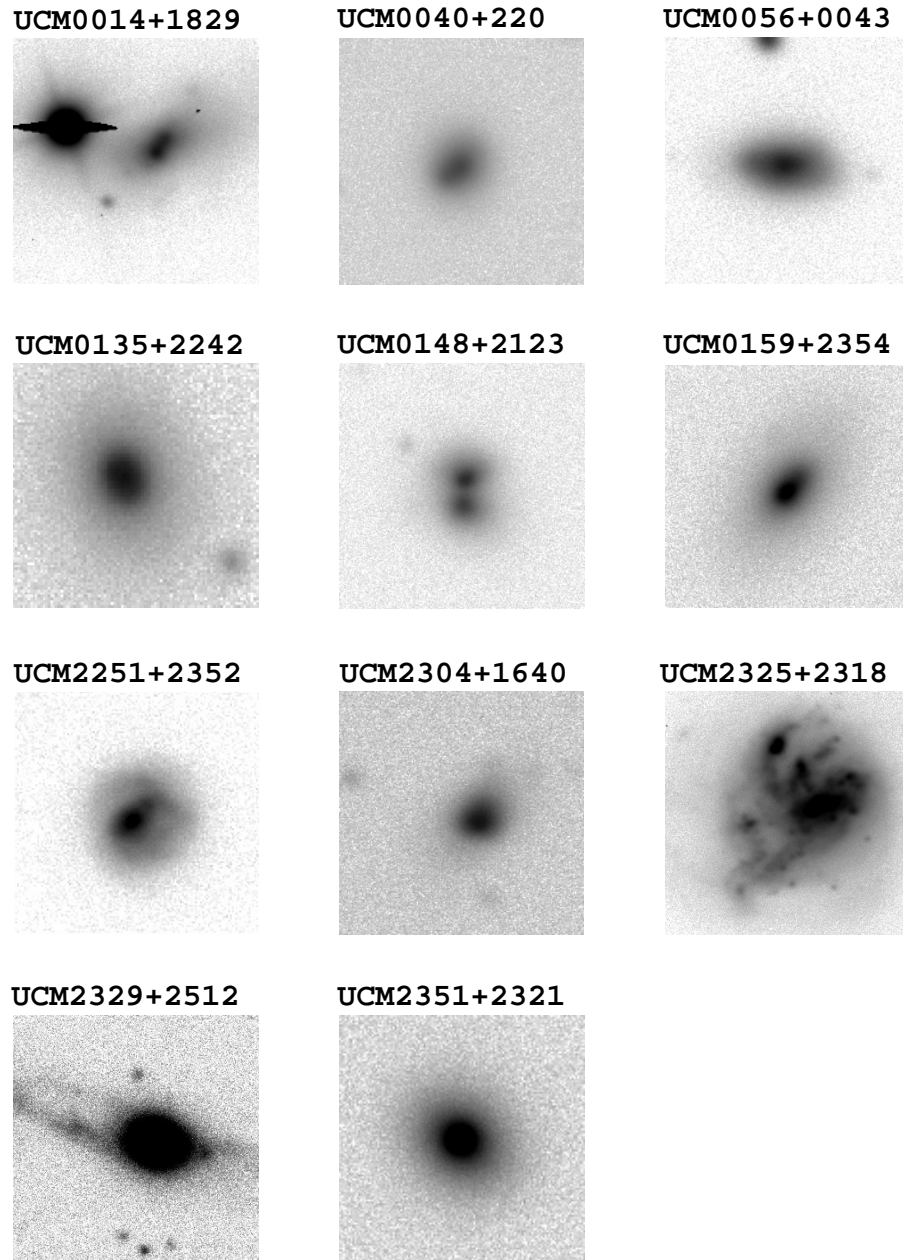


FIG. 4.—R-band logarithmic gray-scale images from the WIYN 3.5 m telescope obtained in $1''.2$ mean seeing. North is up, and images are 10 kpc on a side at the adopted distance of each source.

double-lobed appearance of this galaxy. In addition, this galaxy has one of the smallest τ_{gas} , 0.65 Gyr, meaning it will rapidly use up its $3.8 \times 10^8 M_{\odot}$ of H I. This could be indicative of an ongoing interaction. UCM 0148+2123 has an asymmetric, single-peaked H I profile, which may be caused by two galaxies being observed. As with most of our galaxies, the H II profile is narrower ($W_{20} = 98 \text{ km s}^{-1}$) and more symmetric than the H I profile ($W_{20} = 200 \text{ km s}^{-1}$). The H I profile extends further to lower velocities than the H II profile does, suggesting a difference in the neutral and ionized gas distributions.

4.6. UCM 0159+2354

UCM 0159+2354 features an elongated core and extended, diffuse disk, indicative of a highly inclined system. There may be some small, faint galaxies also in this field,

but it is not at all clear whether they are associated with our target galaxy. While UCM 0159+2354 has a normal R_{eff} , 1.0 kpc, it is the most concentrated galaxy in our sample, 4.25, and is also optically asymmetric, $A = 0.12$. In addition, UCM 0159+2354 is the reddest galaxy in our sample with a $B-r$ color of 1.00. The H I spectrum shows a single-peaked profile for this galaxy. The center of the H II spectrum is offset in velocity from the H I profile (4925 km s^{-1} versus 4901 km s^{-1}). The H II profile is also narrower (138 km s^{-1} versus 192 km s^{-1}). This may indicate a real difference in the distributions of the neutral and ionized gas.

4.7. UCM 2251+2352

There are two galaxies apparent in the H I spectrum of UCM 2251+2352. While both detections have similar widths, the one at higher redshift is significantly brighter

and is our desired target, based on its coincidence with the H II profile. The H I profile is wider than the H II profile (140 versus 79 km s⁻¹), mostly because of high-velocity wings, while the central profiles match quite well. The DSS image shows a few faint galaxies to the south and west of our target galaxy, but it is not clear if this is what we have detected at lower redshift in our H I spectrum. Our WIYN R-band image reveals a very faint, nearly face-on, barred spiral structure. The face-on nature of this galaxy makes any dynamical mass determination highly uncertain because of the large inclination corrections needed. UCM 2251+2352 has a somewhat extended disk with $R_{\text{eff}} = 1.4$ kpc and is relatively concentrated, $C = 3.43$. It is, however, the most asymmetric galaxy in our sample, with $A = 0.27$.

4.8. UCM 2304+1640

UCM 2304+1640 has a bright core, with a faint, extended, diffuse disk surrounding it. The DSS image of the field shows multiple diffuse objects, suggesting that we may have a spectrum of a galaxy group. The half-light radius of UCM 2304+1640 is one of the smallest in our sample at 0.7 kpc. The galaxy is rather concentrated, $C = 3.35$, and asymmetric, $A = 0.12$, as well. This galaxy has a single-peaked H I profile that is somewhat rounded on top; this would be consistent with observing a group of galaxies as seen in the DSS image. The H II profile is more symmetric, narrower, and slightly offset from the peak of the H I profile, also consistent with multiple objects being in the Arecibo beam.

4.9. UCM 2325+2318

Both the WIYN and DSS images of UCM 2325+2318, also known as NGC 7673, clearly shows signatures of interactions, with loops and a tail apparent around the main galaxy. This is the most extended galaxy in our sample, $R_{\text{eff}} = 1.9$ kpc, and not very concentrated, $C = 2.98$. UCM 2325+2318 is also the most asymmetric galaxy we observed, with $A = 0.60$. Conselice et al. (2000a) measured the same A value based on earlier WIYN imaging and noted this galaxy has a large ratio of W_{20} to W_{50} . These authors found that a large value of this ratio was correlated with morphology, indicative of recent interactions. Consistent with this, Gallego et al. (1996) have identified three components in their H II spectrum of this galaxy and have stated that this is an interacting system. Nordgren et al. (1997a) observed the H I disk of this system to be disturbed. NGC 7673 is also a well-known luminous FIR source (Sanders & Mirabel 1996), which is not surprising considering that the SFR is $23.5 M_{\odot} \text{ yr}^{-1}$, yielding $\tau_{\text{gas}} = 0.18$ Gyr. This is the highest SFR and shortest τ_{gas} in our sample. UCM 2325+2318 has a very strong, single-peaked H I profile, which has been studied in detail by Homeier & Gallagher (1999) with spectra from the WIYN DensePak integral field unit. In particular, they have measured the velocity field of this galaxy in the plane of the sky, yielding a better estimate of its rotation velocity, $W_{20} = 126$ km s⁻¹ versus $W_{20} = 119$ km s⁻¹ from our Keck spectrum; a fine agreement. The H II profile is narrower than the H I profile ($W_{20} = 119$ versus 164 km s⁻¹), and the relative positions of the peaks differ by ~ 10 km s⁻¹.

4.10. UCM 2329+2512

The WIYN image of UCM 2329+2512 reveals a very small ($R_{\text{eff}} = 0.6$ kpc), concentrated ($C = 4.15$) galaxy with

a faint, stellar loop, possibly indicative of a recent interaction. Despite this signature of interaction, it is remarkably symmetric, $A = 0.02$. The low asymmetry is because the measurement of asymmetric is only in the central 7" and is dominated by the bright central region and not the faint loops. The faint loops could just be the projection of a strong two-armed spiral pattern in a highly inclined disk and not a tidal tail. The symmetric, double-horned H I profile would support the idea that this system has not been disturbed. UCM 2329+2512 also has a low SFR, and the longest τ_{gas} , 7.3 Gyr, of our sample. No other galaxies are apparent in the DSS image of the Arecibo field. The H II spectrum of this galaxy is completely different from the H I profile, with a symmetric, single-peaked profile. This suggests that the limited star formation in this galaxy is taking place only in the central regions, while the H I is much more extended.

4.11. UCM 2351+2321

We did not detect H I in UCM 2351+2321. The 3σ upper limit on its H I mass is $1.3 \times 10^8 M_{\odot}$ for an assumed width of 160 km s⁻¹ (from the H II spectrum). There is a hint of H I emission near where the H II profile rises at high velocity, but it is too weak to be a definite detection. Optically, UCM 2351+2321 is one of the reddest ($B-r = 0.94$ mag) and most concentrated, $C = 4.02$, targets. In some respects, this is the most interesting galaxy of the entire sample because of the strong H α emission yet weak H I emission, implying a very small gas depletion timescale of < 0.03 Gyr. If any galaxy among our sample represents a transition type between a gas-rich starburst and a gas-poor spheroidal, this may be such an object.

5. DISCUSSION

5.1. Kinematics of Local BCGs

The most interesting feature of our sample is that the ratio of H II to H I 21 cm line widths, $\mathcal{R} = W_{20}(\text{H II})/W_{20}(\text{H I})$, is always below unity. A further examination of the observed H II and H I profiles in Figure 2 shows that all but one of the H II spectra (UCM 0135+2242) and all but two of the H I spectra (UCM 0135+2242 and 2329+2512) are singly peaked, indicative of either extremely face-on disks or solid-body rotation curves commonly seen in H II galaxies (see, e.g., van Zee et al. 1998). The latter option is more likely due to the large velocity widths of the lines, despite being singly peaked.

Figure 5 plots \mathcal{R} versus the H II emission line widths, $W_{20}(\text{H II})$. Filled circles denote galaxies from this paper, while crosses denote the spiral and irregular galaxies studied by Kobulnicky & Gebhardt (2000); triangles denote the spiral sample of Raychaudhury et al. (1997), and squares are the H II galaxies from Telles & Terlevich (1993). It is evident from the figure that the H II–H I line width ratio systematically departs from unity for small H II line widths. This effect is most prevalent for galaxies with $W_{20}(\text{H II}) \leq 200$ km s⁻¹. The compact galaxies from our paper show a systematic difference between the neutral and ionized gas kinematics such that they have a mean $\mathcal{R} = 0.66 \pm 0.16$, which is different from most normal galaxies with a ratio closer to 1. Our galaxies are similar, in this respect, to the H II galaxies and H II regions studied by Telles & Terlevich (1993), which have line width ratios of $\sigma_{[\text{O III}]}/\sigma_{\text{H I}} \sim 0.7$. Figure 5 illustrates that this discrepancy between the H II

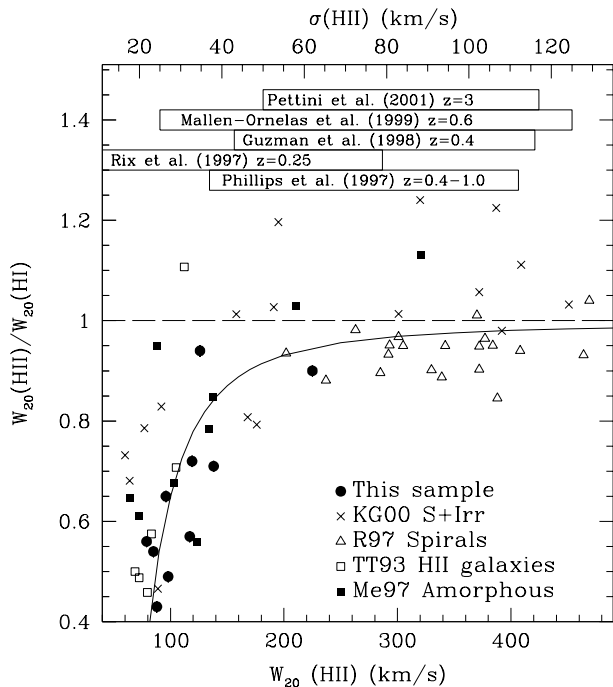


FIG. 5.—Comparison of the observed H II line widths (i.e., not corrected for inclination) vs. the ratio of H II-to-H I line widths. Filled circles denote our sample, crosses denote the sample of spiral and irregular galaxies studied by Kobulnicky & Gebhardt (2000), open triangles denote the spiral sample of Raychaudhury et al. (1997), and open squares are the H II galaxies from Telles & Terlevich (1993) with H I widths as measured by Smoker et al. (2000). The measured H II-to-H I ratio departs systematically from unity for galaxies with small H II line widths. The solid line is an approximate fit to the data: $W_{\text{HII}}/W_{\text{HI}} = 1 - 5W_{\text{HII}}^{-1} - 500W_{\text{HII}}^{-2} - 2.5 \times 10^5 W_{\text{HII}}^{-3}$. The boxes at the top of the figure illustrate the range of velocity widths measured for compact galaxies in the HDF-f (Phillips et al. 1997), $z \sim 0.6$ field galaxies (Mallén-Ornelas et al. 1999), $z \sim 0.25$ field galaxies (Rix et al. 1997), and compact blue galaxies at $z \sim 0.4$ (Guzmán et al. 1998). Our sample of compact blue galaxies have $W_{\text{HII}}/W_{\text{HI}} \sim 0.6$, similar to the ratio for H II galaxies studied by Telles & Terlevich (1993). This effect is capable of reducing the T-F offsets found at intermediate redshifts by some studies.

and H I line widths seems to vary smoothly from large line widths to small. Therefore, we have attempted to quantify this effect for all galaxies through an approximate polynomial fit to the data as follows:

$$\mathcal{R} = W_{\text{HII}}/W_{\text{HI}} = 1 - 5W_{\text{HII}}^{-1} - 500W_{\text{HII}}^{-2} - 2.5 \times 10^5 W_{\text{HII}}^{-3}. \quad (3)$$

This equation yields a very rapid drop-off in \mathcal{R} below $W_{20}(\text{H II}) = 100 \text{ km s}^{-1}$, which becomes unphysical below $W_{20}(\text{H II}) = 68 \text{ km s}^{-1}$. Since we have not observed \mathcal{R} values below 0.4, we suggest that when applying the above formula, a lower bound of 0.3 is imposed.

Note that there is still a large scatter around this fit, so this formula should be applied with great caution. A likely interpretation of the data is that the optical emission lines trace a smaller portion of the gravitational potential than the H I does, particularly in those galaxies with the smallest line widths (i.e., $\sigma < 40 \text{ km s}^{-1}$). For these galaxies, the dynamical masses based on the width of optical emission lines will underestimate their masses by factors of 2–4. However, for galaxies with velocity widths, σ , larger than $\sim 40 \text{ km s}^{-1}$ the effect on the mass estimates is only less than 20%.

In addition to the observed dependence on velocity width, we have attempted to find a set of observational parameters that can identify galaxies in which the line width ratio, \mathcal{R} , is small. While we searched for correlations between all the observed parameters (color, SFR, concentration, asymmetry, R_{eff} , SBe, etc.) and the line width ratio, we had limited success. In Figure 6, we plot the relation between the line width ratio, H α equivalent width, and concentration index; NGC 4449 is plotted as a comparison object. Only the bottom panel shows any hint of a correlation: objects with higher EW (H α) seem to have lower line width ratios, while those with lower EW (H α) have a wider range of ratios. The relation, really an upper envelope, between EW (H α) and \mathcal{R} may indicate that galaxies undergoing a large starburst have small line width ratios. Physically, this could be caused by a minor merger driving some gas into the center of a galaxy, triggering a central starburst (see, e.g., Hernquist & Mihos 1995). Therefore, most of the line emission will be centrally concentrated, while the H I disk will be more extended. Such a starburst cannot dominate the optical light, however, since there is no correlation between the line width ratio or EW (H α) and concentration index. Alternatively, some of the H I gas could be in the process of being ejected from the galaxy and is no longer tracing the gravitational potential. This would require very large amounts of mass to be ejected without being ionized. Furthermore, the shapes of most of the H I profiles can be more simply explained by galactic rotation than by ejection.

5.2. Neutral Gas Masses and the Potential For Future Star Formation

The 10 galaxies with 21 cm detections have H I masses ranging from $0.26\text{--}4.3 \times 10^9 M_{\odot}$. This H I mass range is typical for later-type spiral (Sc-Sm) and irregular galaxies (Roberts & Haynes 1994). The SFRs of our 10 sample galaxies range between $0.23\text{--}23.5 M_{\odot} \text{ yr}^{-1}$. Thus, our sample spans a wide range of H I masses and H α luminosities (or SFRs) similar to the heterogeneous sample of spiral galaxies studied by Kennicutt, Tamblyn, & Congdon (1994, hereafter KTC), as shown in Figure 7. The gas depletion time-scales for our sample of galaxies are also similar to the KTC sample, with typical $\tau_{\text{gas}} > 1 \text{ Gyr}$, also shown in Figure 7. Only three to four galaxies in our sample have τ_{gas} less than 1 Gyr: UCM 0040+0220, 0148+2123, 2325+2318, and 2351+2321. These are not anomalously low for KTC spirals, but they are on the lower edge of the distribution. The cause of these low τ_{gas} values is either having a small H I mass and a moderate SFR (see, e.g., UCM 0040+0220 and 0148+2123) or a high SFR and moderate M_{HI} (see, e.g., UCM 2325+2318) or a combination of high SFR and low M_{HI} (see, e.g., UCM 2351+2321).

From the inclination-corrected H I line widths, we estimate the dynamical mass of each system using R_{HI} as a fiducial radius. The masses range from 3.7×10^9 to $1.5 \times 10^{10} M_{\odot}$. It should be noted that the derived inclinations can be highly uncertain ($\pm 15^\circ$) and can produce large corrections to the H I line widths for low inclinations. Such errors in inclination propagate into our mass determination as the square of the line width. If our estimate of $R_{\text{HI}} = 4.5R_{\text{eff}}$ is too large, then the dynamical masses should be reduced in proportion to R_{HI} .

Using our derived M_{dyn} and calculated M_{HI} , we can calculate the neutral hydrogen gas mass fraction, f_{gas} . The gas mass fractions for our sample have reasonable values that

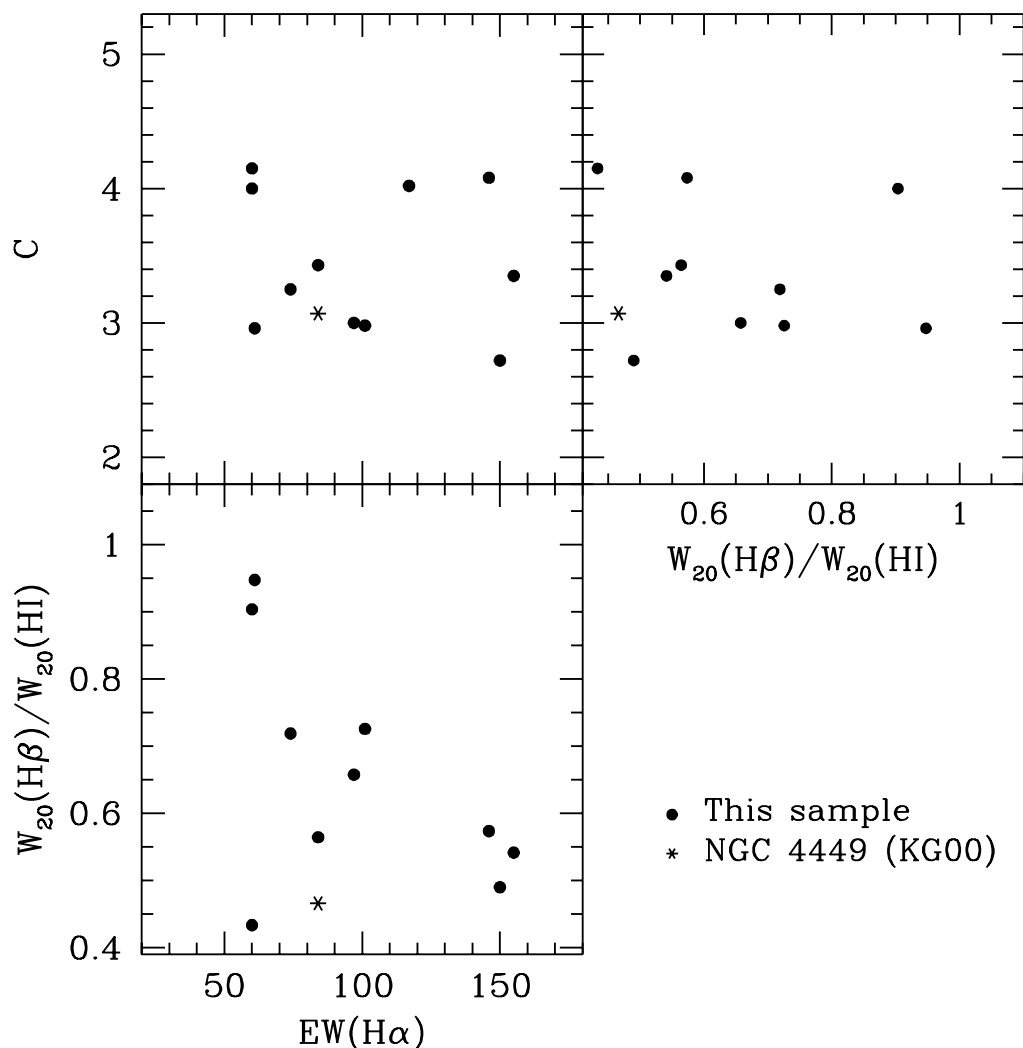


FIG. 6.—Diagnostic parameters of the nearby galaxy sample (*filled circles*), illustrating the relation between line width ratio, $[W_{20}(\text{H}\beta)/W_{20}(\text{H}\text{I})]$, H α equivalent width, EW (H α), and concentration index, C . The nearby irregular galaxy NGC 4449, marked by an asterisk, is included as a comparison object. Objects with high EW (H α) tend to have the smallest H β and/or H I line widths, although the dispersion is large.

range from 0.01 to 0.54, with a mean value of 0.12. Thus, some of these galaxies may be gas-rich like nearby H II and irregular galaxies ($f_{\text{gas}} \sim 0.3\text{--}0.5$; van Zee et al. 1998), while others could have gas mass fractions typical of the Milky Way and other spirals ($f_{\text{gas}} < 0.10$; Roberts & Haynes 1994).

There are some ambiguities in the interpretation of H I profiles worth consideration. Our estimates of H I masses may be too large if there are multiple galaxies in the relatively large Arecibo beam (90 kpc in extent at an average distance of 83 Mpc). Multiple galaxies are not necessarily easy to identify from a spatially integrated H I profile. They can produce asymmetric single- or double-peaked profiles, and/or flat- or round-topped H I profiles (see Nordgren et al. 1997a, 1997b for examples). Depending on the masses and dynamics of the system, the asymmetries may be quite small, even if the relative masses are high. An overestimate of the H I masses would result in an overestimate of τ_{gas} . Therefore, these galaxies may be using up their H I at a more prodigious rate than indicated by the present estimates. Finally, it is difficult to determine if interactions are ongoing in the sample galaxies from the H I profiles. Interactions will affect the observed line widths and, hence, the accuracy of our calculated dynamical masses. Strong single

peaks are predicted and seen in some merger remnants (Horellou & Booth 1997; Bendo & Barnes 2000), but other interacting systems or merger remnants are indistinguishable from normal, isolated galaxies (Horellou & Booth 1997). Only with higher spatial resolution H I observations can these ambiguities be cleared up. For this paper, we can only assume that we have observed single galaxies.

5.3. Comparison with Intermediate-Redshift BCGs

Over the last few years, there has been an increasing controversy surrounding the reliability of the virial mass estimates using velocity widths measured from ionized gas emission in BCGs at intermediate redshifts. It is well known that the ionized gas does not always sample the whole range of the rotation curve, since the space distribution of the ionized gas is typically more compact than the extended H I (see, e.g., Broeils 1992; Taylor et al. 1995). Velocity widths derived using ionized gas emission lines likely underestimate the actual galaxy gravitational potential and thus the inferred virial mass. The key question is how do we relate optical line widths to the rotation velocity? Since emission-line velocity widths are often used to estimate galaxy masses in unresolved BCGs at higher redshifts, it is important to

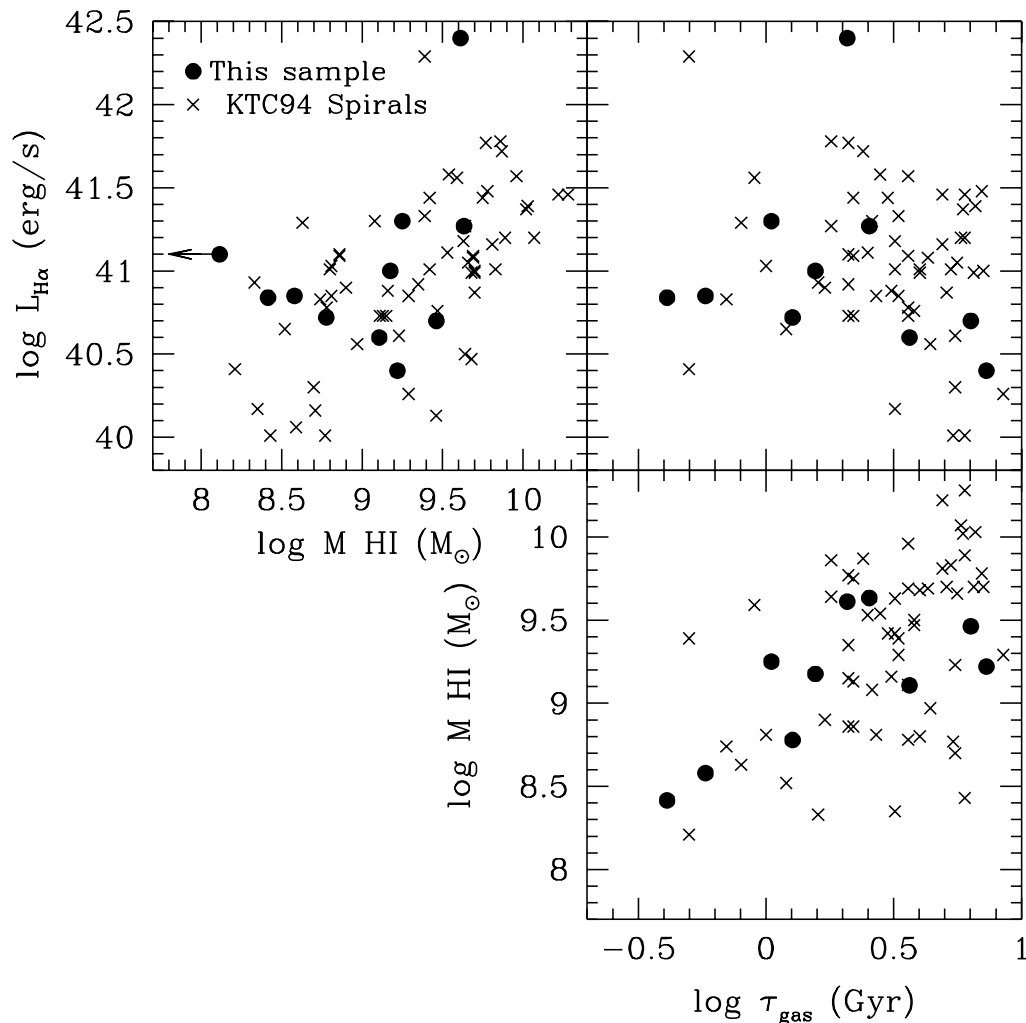


FIG. 7.—Comparison of M_{HI} and $L_{\text{H}\alpha}$ (top left), τ_{gas} and $L_{\text{H}\alpha}$ (top right), and M_{HI} and τ_{gas} (bottom right) for the UCM BCG analogs (filled circles) and a sample of spiral galaxies from Kennicutt et al. (1994; crosses). It is evident that the two samples of galaxies occupy a similar region of parameter space in all three plots, although a couple of UCM galaxies do have much shorter τ_{gas} than the Kennicutt et al. (1994) sample. The upper limit of M_{HI} and τ_{gas} for UCM 2351 + 2321 is off the left side of the plot.

assess the degree at which these measurements may be biased by a likely underestimation of the actual rotation velocity.

For BCGs at redshifts of $z < 0.35$, the issue was first discussed by Guzmán et al. (1996), who reanalyzed \mathcal{R} in the published data for a sample of nearby H II galaxies (Telles & Terlevich 1992) and concluded that “since CNELGs are similar to H II galaxies, the measured velocity widths are likely to underestimate their internal velocities by as much as 30%.” A 30% increase was thus applied to velocity width measurements in subsequent papers (see, e.g., Guzmán et al. 1998). The value of this correction was also investigated by Rix et al. (1997), who compared the velocity dispersion in the ionized gas, σ_v , with the maximum circular velocity of the ionized gas, V_c , for three, well-resolved, nearby galaxies. They found an average value of $\sigma_v/V_c = 0.6$, which is consistent with the analytic prescription of Tully & Fouqué (1985). On the other hand, Lehnert & Heckman (1996) showed a very poor correlation between emission-line velocity widths and rotational velocities for a sample of local starburst galaxies (see their Fig. 13). They noted that emission lines from nuclear regions trace only a fraction of the rising portion of the rotation curve in nuclear star-

bursts, but they did not investigate how this affected the spatially integrated optical spectrum of the galaxy or how global optical line widths compared with the H I line widths. Neither Rix et al. (1997) nor Lehnert & Heckman (1996) discussed the relation of the ionized gas kinematics to the neutral gas kinematics, which is the issue of interest here. Kobulnicky & Gebhardt (2000) performed integrated optical spectroscopy of 21 galaxies, including some of the Lehnert & Heckman (1996) nuclear starburst sample, and they found good agreement between optical and H I line widths for all objects except NGC 4449. Note that NGC 4449 is the object in the Kobulnicky & Gebhardt (2000) sample that most closely resembles the BCG population.

In order to assess the relevance of our work for distant galaxies, it is important to consider how analogous our sample of 11 galaxies is to the intermediate-redshift BCGs that we wish to learn more about. We can examine how our sample galaxies compare in the M_B - $\sigma_{\text{H II}}$ and R_{eff} - $\sigma_{\text{H II}}$ planes. In Figure 8, we compare the distribution of our sample galaxies with the BCGs of Phillips et al. (1997) and Guzmán et al. (1998). While our galaxies span nearly the full range of M_B and R_{eff} as the distant BCGs, they have systematically smaller line widths. Indeed, the nearby sample

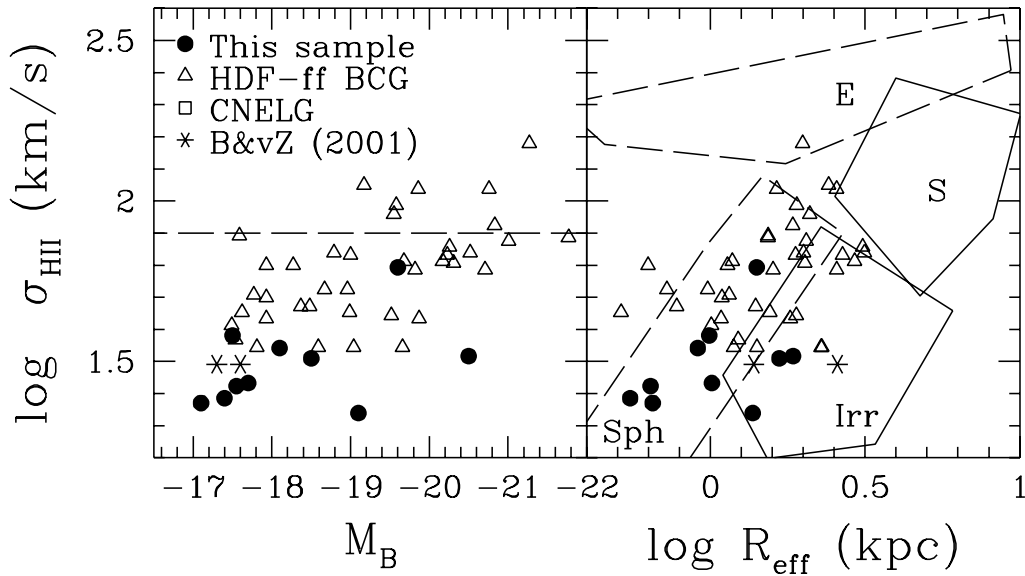


FIG. 8.—Comparison of the sample galaxies (*filled circles*) with the same intermediate-redshift BCGs (*squares and triangles*) from Fig. 1. The left panel compares the velocity dispersion with absolute blue magnitude (M_B). The right panel compares the emission-line velocity dispersion, σ_{HII} (not corrected for inclination), with the logarithm of the effective radius (R_{eff}). The velocity dispersion is measured via the $\text{H}\beta$ line for our sample and via a combination of $\text{H}\beta$, $[\text{O II}]$, and $[\text{O III}]$ line widths for the intermediate-redshift BCGs. Our sample galaxies have smaller velocity dispersions than the intermediate-redshift BCGs, on average.

shows a mean emission-line velocity width near 30 km s^{-1} compared with $50\text{--}60 \text{ km s}^{-1}$ for the BCGs; both sets of line widths are uncorrected for inclination. Figure 8 brings into question whether we are truly observing analogs to the intermediate-redshift BCGs. We believe, however, that our sample galaxies, while not representative of all intermediate-redshift BCGs, are similar to those with the smallest line widths (i.e., $\sigma < 40 \text{ km s}^{-1}$).

The hypothesis that we are observing analogs to at least some of the intermediate-redshift BCGs is supported by examining other morphological and photometric properties of our galaxies. In Figure 9, we plot the $B-V$ colors versus asymmetry, A , concentration index, C , and B -band surface brightness with the half-light radius, SBe , for our sample galaxies, the Frei (1999) sample of local, luminous elliptical and spiral galaxies with parameters measured by Bershady, Jangren, & Conselice (2000), the luminous BCG sample from Jangren et al. (2001), and the BCG sample from the HDF-ff with parameters measured by Guzmán et al. (1997). With the exception of two red sources (UCM 0159+2354 and 2351+2321), our galaxies occupy a location in the $B-V$ versus SBe and $B-V$ versus C planes that overlaps strongly with the intermediate-redshift BCG samples and is clearly distinct from normal, nearby galaxies. Most of the galaxies in our sample are less luminous and redder than the majority of the intermediate-redshift BCGs. Based on the definition of BCGs from Jangren et al. (2001), seven of our 11 galaxies are “BCGs” (the exceptions are UCM 0148+2124, 0159+2354, 2329+2512, and 2351+2321). Of those seven, only the three most luminous galaxies in our sample technically fit the “LBCG” definition of Jangren et al. (2001; UCM 2325+2318, 0135+2242, and 2251+2352). All these points serve to illustrate that we must be very careful about what we infer regarding the nature of intermediate-redshift BCGs based on observations of our sample of galaxies or similar samples in the local universe. For instance, the two nearby galaxies Barton & van Zee

(2001) propose are local counterparts to the intermediate-redshift BCG population would not have been selected as such by the color–surface brightness criteria defined by Jangren et al. (2001). These two nearby galaxies are either redder or of lower surface brightness (or both) than the intermediate-redshift BCGs, as well as the nearby sample studied here. With this caveat in mind, we will now examine what we can learn about intermediate-redshift BCGs.

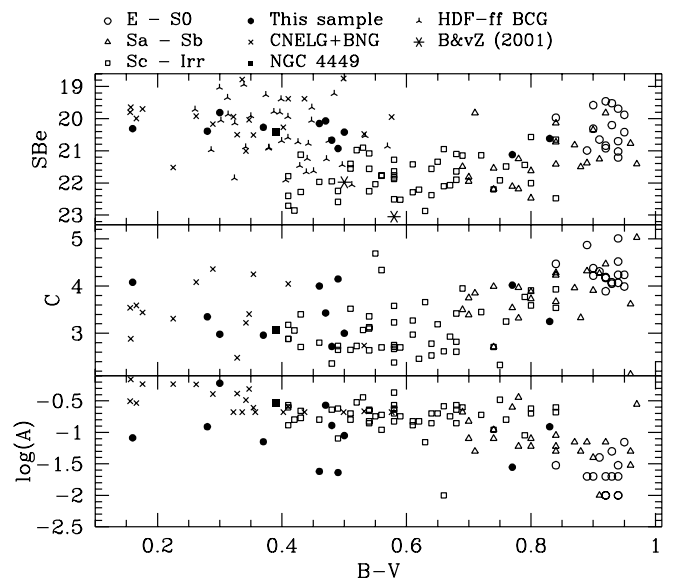


FIG. 9.—Diagnostic parameters including color ($B-V$), B -band surface brightness (SBe in mag arcsec^{-2}), concentration index (C), and asymmetry (A). Filled circles denote our sample, and open symbols denote nearby galaxies from the Frei (1999) catalog taken from Bershady et al. (2000). Crosses and upside-down Y’s denote the BCG collection of Jangren et al. (2001). Note that our sample of nearby compact galaxies shares a unique space in these diagrams with the intermediate-redshift BCGs, indicating that analogs of the intermediate-redshift compact galaxies can be found among our sample.

At the top of Figure 5, we have drawn several boxes to represent the range of line widths for the galaxies in the studies of the HDF-ff (Phillips et al. 1997), $z \sim 0.6$ field galaxies (Mallén-Ornelas et al. 1999), $z \sim 0.25$ field galaxies (Rix et al. 1997), and compact blue galaxies at $z \sim 0.4$ (Guzmán et al. 1998). Figure 5 shows that the discrepancy between H II and H I line widths described in § 4.1 could affect the mass determinations in all these studies. The effect can be as much as a factor of 2–4 for the smallest velocity width galaxies. However, according to our empirical relation, the effect may be only $\sim 30\%$ – 40% for galaxies with velocity widths $\sigma > 40 \text{ km s}^{-1}$. Note that this effect is in addition to other well-recognized uncertainties in mass determinations due to unknown inclinations and clumpy gas distributions (modeled for spiral galaxies by Rix et al. 1997). A more rigorous approach to apply the results from our study to the intermediate-redshift BCG population is to restrict our conclusions to only the seven galaxies that can be considered “bona fide” counterparts according to Jangren et al.’s definition. These galaxies have an \mathcal{R} ranging from 0.54 to 0.94, with a mean value of 0.70. The three bona fide LBCG counterparts have essentially the same mean and range. For the three non-BCG galaxies we detected in H I, the mean value of \mathcal{R} is only 0.54. These values of \mathcal{R} for BCGs are in good agreement with the corrections applied to the mass estimates in previous work at higher redshift (see, e.g., Guzmán et al. 1996, 1998).

One of the most interesting conclusions derived using mass estimates of BCGs at intermediate redshifts is that their mass-to-light ratios are roughly 1 order of magnitude lower than those values characteristic of local galaxies with similar luminosities (Guzmán et al. 1996; Phillips et al. 1997). This conclusion can be tested with our sample of nearby BCGs. For consistency with previous work, we define the mass-to-light ratio within R_{eff} (instead of R_{H}), using the velocity dispersion of the H I and uncorrected by inclination effects. This definition allows a direct comparison with values published in the literature for a wide variety of galaxy types. For our entire sample, the derived mass-to-light ratios range from 0.07 to $0.78 M_{\odot}/L_{\odot}^B$. The mean mass-to-light ratio for non-BCGs, $0.6 M_{\odot}/L_{\odot}^B$, is higher than for the BCGs, $0.3 M_{\odot}/L_{\odot}^B$, in our sample. These values are consistent with the mass-to-light ratios for the intermediate-redshift BCGs studied by Phillips et al. (1997). The mean absolute magnitude is $M_B = -19.2$ mag, about 1.3 mag fainter than L_* . Using the same representative sample of local galaxies in the Third Reference Catalog of Bright Galaxies (RC3; de Vaucouleurs et al. 1991) analyzed by Phillips et al. (1997), we estimate that nearby, “normal” galaxies with $M_B \sim -19.2$ have mass-to-light ratios that approximately range from 0.8 to $10 M_{\odot}/L_{\odot}^B$. The observed range in mass-to-light ratios for BCGs is inconsistent with that characteristic of massive systems with comparable luminosities, such as Sa-Sc spiral galaxies. These spirals tend to be the most abundant galaxy type with this luminosity in the local universe. Instead, BCGs have mass-to-light ratios that are similar to the lowest observed values in lower mass galaxies of similar luminosity, such as irregulars and H II galaxies. As our BCG counterparts evolve, their mass-to-light ratios will increase to values more comparable to normal, spiral galaxies, provided that they fade.

Finally, the observed distribution of gas depletion timescales, τ_{gas} , provides additional information about the nature and evolution of the distant BCG galaxy population.

Of the seven BCGs in our sample, two have $\tau_{\text{gas}} < 0.5$ Gyr, two have $\tau_{\text{gas}} \sim 1$ Gyr, and three have $\tau_{\text{gas}} > 2$ Gyr. The wide range observed suggests a very heterogeneous population of objects with very different burst strengths and reservoirs of neutral gas. The BCGs with the smallest gas depletion timescales will shortly cease star formation and thus may be good candidates to undergo subsequent passive evolution. However, a long period of passive evolution following the end of the current starburst in BCGs with $\tau_{\text{gas}} > 2$ Gyr seems less likely, and these galaxies may continue having subsequent events of star formation.

5.4. Implications for the Evolution of the T-F Relation

A related controversy exists concerning whether velocity widths of ionized gas are suitable for the study of galaxy scaling relations such as the T-F relation (Tully & Fisher 1977). Traditionally, the T-F relation is a correlation measured between luminosity and H I line width. It has been well established that “terminal” rotation speeds derived from spatially resolved velocity fields (in the optical or H I) provide a well-defined surrogate for H I line widths for normal spiral galaxies in the local universe (see, e.g., Mathewson, Ford, & Buchhorn 1992; Courteau 1997). Ionized gas line widths are of particular interest for intermediate- and high-redshift work, where spatial resolution and signal-to-noise are limited and H I is out of reach with present telescopes and instrumentation. However, there has been only limited exploration of whether optical *line widths* are suitable surrogates for use in measuring the T-F relation (see, e.g., Rix et al. 1997; Kobulnicky & Gebhardt 2000). Despite this fact, there have been a number of studies attempting to exploit the observability of optical line widths for drawing inferences about the evolution of the mass-to-light ratios of intermediate-redshift galaxies, as discussed in § 1. Our purpose here is to demonstrate that these results should be viewed with caution.

Figure 10 shows how our sample of compact galaxies compares with the T-F relation. Each galaxy in our sample is plotted three times. Dotted circles denote the measured H II line widths, $W_{20}(\text{H II})$, open circles denote the measured H I 21 cm line widths, $W_{20}(\text{H I})$, and filled circles denote the inclination-corrected H I 21 cm line widths, $W_{20}(\text{H I})/\sin i$. For comparison, we also plot H II galaxies from Telles & Terlevich (1993; *crosses*) and the B-band T-F relation of Pierce & Tully (1988; *solid line*).⁷ While the compact galaxies in our sample lie near the relation for H II galaxies and show a large offset from the canonical T-F relation when using observed H II line widths, if we adopt the inclination-corrected H I widths, our sample is consistent, on average, with the T-F relation for normal galaxies.

Prompted by this result, we have reexamined the results of T-F studies at intermediate redshift employing line widths. Specifically, we have recomputed magnitude offsets from T-F for the Forbes et al. (1996), Rix et al. (1997), and Mallén-Ornelas et al. (1999) samples after applying the line width correction in equation (3) (Fig. 5). The line widths of

⁷ $M_B = -6.86 \log(V_M) - 2.27$. In order to convert V_M to the observed quantity, W_{20} , we adopt the prescription of Tully & Fouqué (1985), $(2V_M)^2 = W_R^2 = W_{20}^2 + W_t^2 - 2W_{20}W_t[1 - e^{-(W_{20}/W_t)^2}] - 2W_t^2 e^{-(W_{20}/W_t)^2}$. Here W_R is the rotation full amplitude, which is $2V_M$, $W_t = 38 \text{ km s}^{-1}$ is the width due to turbulent motions, and $W_c = 120 \text{ km s}^{-1}$ is the transition point between galaxies having Gaussian and those having double-horned H I profiles.

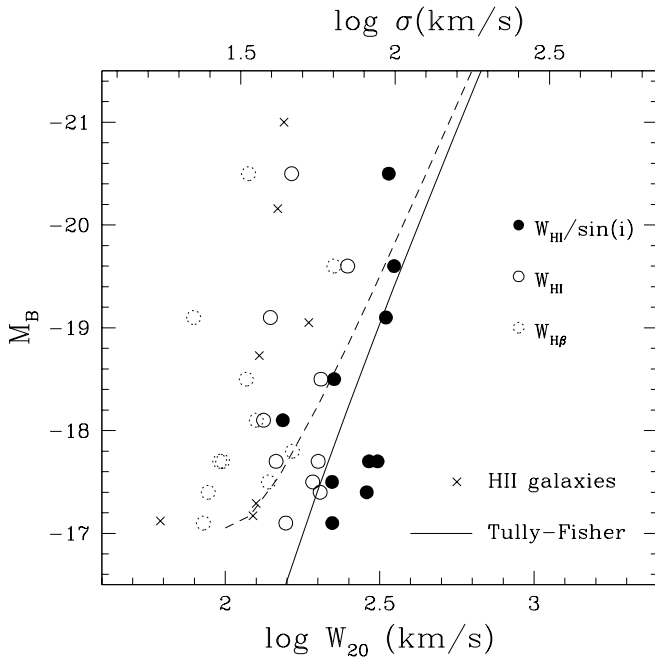


FIG. 10.—Comparison between our sample galaxy kinematics (*circles*), H II galaxies (*crosses*) from Telles & Terlevich (1993), and the canonical T-F relation [*solid line*; $M_B = -6.86 \log(W_R) - 2.27$ from Pierce & Tully 1988]. The raw H II velocity widths (*dashed circles*) for our sample are most consistent with the locus of the H II galaxies. The H I velocity widths (*open circles*) are closer to the T-F relation. However, the inclination-corrected H I velocity widths (*filled circles*) are consistent with the T-F without any luminosity offsets. The dashed curve shows how the T-F relation would be modified if measured using inclination-corrected optical line widths, based on the relation adopted in Fig. 5.

the Forbes et al. sample are such that corrections based on our formulation are minimal, despite the discussion noted above, based on their own rotation curve data. Indeed, it is sobering to note that of the two galaxies for which they have rotation curves, the galaxy with the small line width correction appears to have a bimodal light distribution, while the galaxy with the large line width correction appears to be a relatively normal spiral with large luminosity and size (see their Fig. 1).

For Rix et al., we use their tabulated line widths and adopt the Pierce & Tully (1988) T-F relation, which has a slope of $\gamma = -6.86$. The adopted slope is within 1σ of the value derived by Rix et al. (1997) for their intermediate-redshift sample; ours is a conservative choice, since their mean slope is much steeper ($\gamma = -14.3$) and, hence, results in much larger magnitude-offset corrections. We find a mean offset of -1.8 mag without applying a line width correction. This is -0.3 mag larger than their quoted mean value, consistent with our ignoring the color dependence to the T-F zero point (see their § 3.3.1, eq. [9]). However, with line width corrections, we find a mean offset of -1.1 mag, or $+0.7$ mag less brightening than estimated by Rix et al. (1997). Accounting for their color dependence results in a net corrected brightening of -0.8 mag in the T-F zero point at $z \sim 0.25$.

To make a fair reassessment with Mallén-Ornelas et al.'s results, we adopt their T-F slope of $\gamma = -7.46$. Since Mallén-Ornelas et al. (1999) do not provide tabulated data nor a zero point for their fiducial T-F relation, we estimate a correction for their median line width (60 km s^{-1}) estimated from their Figure 2 and calculate a differential correction,

ΔM_c , given as

$$\Delta M_c = -\gamma \log(W_{\text{HI}}/W_{\text{HI}}), \quad (4)$$

where the line width ratio is given by our equation (3). We find the median correction is $+0.2$ mag, although we note that at the lower line width limit of their sample the correction is $+1.9$ mag, which is comparable (but opposite in sign) to their average estimated brightening.

In isolation, the picture that emerges from this reanalysis of intermediate-redshift line width studies is that the evolution of the T-F zero point is more gradual than previously suggested—even for the bluest galaxies studied by Rix et al. (1997) and Mallén-Ornelas et al. (1999). For these galaxies, we estimate -0.8 mag at $z \sim 0.25$ and -1.8 mag at $z \sim 0.6$. However, even this revised estimate should still be tempered by the fact that corrections for color dependence in the T-F relation and inclination are uncertain. For example, the color dependence of the T-F zero point estimated by Rix et al. is ~ 3 times smaller than what is reported in Bershadsky & Andersen (2001). In the absence of direct inclination measurements (e.g., b/a), Rix et al. (1997) have performed an elegant estimate of the mean inclination of their sample. They take into account that the bluest galaxies may preferentially lie at relatively low inclinations (where internal reddening is minimized). However, our sample's mean inclination is 43° , with a maximum of 60° ; almost all our sample is more face-on than the mean inclination of $\sim 57^\circ$ adopted by Rix et al. (1997). If our sample is representative of the inclination distribution of the blue galaxy population, taking into account this change in mean projection results in $+0.6$ mag less brightening (assuming $\gamma = -6.86$). Similarly, Mallén-Ornelas et al. (1999) compare their uncorrected velocities for intermediate-redshift galaxies with a local sample from the RC3. While they make identical cuts in b/a (less than 0.8), the two samples may not have comparable inclination distributions. Our arguments here are admittedly tentative and are not intended to diminish the pioneering efforts made to measure the T-F relation at intermediate redshifts. Yet the striking fact remains that most intermediate-redshift studies employing spatially resolved rotation curves find less evolution (see, e.g., Vogt et al. 1996, 1997; Bershadsky et al. 1999) and that by using the inclination-corrected H I line widths, even the galaxies studied in this paper fall squarely on the local T-F relation.

A corollary to the result in Figure 10 is that our local sample of BCGs cannot fade nor brighten dramatically and remain on the T-F relation. The relatively large reservoir of gas in most of these systems indicates these galaxies will likely experience star formation in their future, as discussed in previous sections. However, the amplitude of past and future star formation is not well constrained, and so the basic assumption that these systems remain (or have been) on the T-F relation is weak. Analogous galaxies at intermediate redshift will also be so weakly bound. Nonetheless, if we assume these galaxies have remained on the T-F relation (or brighter) over lifetimes in excess of 5 Gyr, then the current burst makes only a small contribution to the total stellar mass. Consequently, in this scenario these galaxies also are not candidates for strong fading in the future.

However, it is important to stress that the extant characteristics of the local galaxies studied here are dissimilar to the extreme LBCGs for which a strong fading scenario was originally proposed by Koo et al. (1995) and Guzmán et al. (1996). The fading these authors postulated was part of a

transformation process whereby some subset of the LBCGs evolved into today's spheroidals. As such, these LBCGs would not be expected to lie or remain on the T-F relation at any time. In other words, the assumption that these galaxies must remain on the T-F relation, made in the previous paragraph, is not valid in this scenario.

Finally, the trends of our line width ratio, \mathcal{R} , with line width also has implications for the line widths of Lyman break galaxies (LBGs) observed at $z > 2.7$ (see, e.g., Pettini et al. 2001). Pettini et al. are skeptical of whether their ionized gas line widths are tracing mass. They note, for instance, that they find little evidence for a line width luminosity relation in their sample or in a larger sample at $z \sim 1$. The effect of the line width dependence of \mathcal{R} will be to decrease the slope of the T-F relation, as shown in Figure 10. While the effect is rather mild in Figure 10, it may be more extreme for galaxies at higher redshift. It is striking that while the LBGs are 1–3 mag brighter than the intermediate-redshift LBCGs, they have a comparable range of ionized-gas velocity widths, with mean values of 70 and 60 km s⁻¹, respectively. Indeed, the gas content of galaxies is presumably larger at higher redshifts, and hence it may be reasonable to expect that the value and trend of \mathcal{R} with line width evolves and becomes more extreme at higher redshift. We share then Pettini et al.'s caution in interpreting their ionized gas line widths but remark that our corrections should at least provide a lower limit to what should be applied to the ionized gas line widths at high redshift.

6. CONCLUSIONS

The present sample of compact galaxies were chosen to be analogous to the BCGs at intermediate redshift, so that we could infer the gaseous properties of such galaxies. For our sample, we find that the neutral hydrogen masses, hydrogen gas mass fractions, SFRs, and gas depletion timescales are comparable to nearby gas-rich spiral, irregular, and H II galaxies. The broad range of H I properties imply that BCGs form a very heterogeneous galaxy class. Our sample galaxies have substantial amounts of neutral hydrogen ($\sim 10^9 M_\odot$) and large inferred total masses ($\sim 10^{10} M_\odot$). However, unlike most nearby, luminous spiral and irregular galaxies, the ratio of H II to H I line widths, \mathcal{R} , is systematically less than unity with a mean value near 0.66. In this respect, our sample is similar to nearby H II galaxies. The magnitude of \mathcal{R} is close to what was assumed by Guzmán et al. (1998) and others for intermediate-redshift BCGs. In addition, \mathcal{R} varies with the H II line width, departing dramatically from unity for $W_{20}(\text{H II}) \leq 200 \text{ km s}^{-1}$. We have parameterized this relationship to help those who wish to attempt a correction in higher redshift data. Unfortunately, there is no tight correlation between any of the morphological or photometric properties of these galaxies and the line width ratio, \mathcal{R} . The upper limit of \mathcal{R} does appear to decrease with increasing H α equivalent width, suggesting that this effect is related to central starbursts in these galaxies, but this is a tenuous conclusion. Applying the corrections due to inclination and converting from H II to H I line widths for our galaxies moves them onto the T-F relation, leaving little room for these galaxies to fade if they are to remain on the relation. This implies that the evolution of the T-F relation from intermediate redshift to the present day is smaller and more gradual than has been previously suggested (see, e.g., Rix et al. 1997).

Although the luminosities, colors, and effective sizes of our sample were chosen to mimic those of the BCG population at intermediate redshifts, our sample remains heterogeneous and only samples a portion of the properties of BCGs. Of the 11 galaxies we observed, only seven can be classified as BCGs based on the definition of Jangren et al. (2001). Only the brightest four of those seven BCGs are classified as LBCGs. Furthermore, our galaxies have systematically smaller line widths than the observed population of intermediate-redshift BCGs. They also tend to have, on average, at a given luminosity, smaller sizes. Therefore, our sample is not representative of all intermediate-redshift BCGs but only a subset of them. As such, we are limited in what we can infer regarding the properties of the distant BCGs. For those intermediate-redshift BCGs with small velocity widths and sizes, we can assume that they will also form a heterogeneous population of relatively gas-rich galaxies ($\sim 10^9 M_\odot$), whose gas fractions ($f_{\text{gas}} = 0.02\text{--}0.5$) and gas depletion timescales ($\tau_{\text{gas}} = 0.2\text{--}6 \text{ Gyr}$) may span well over 1 order of magnitude. Although it is not possible to constrain the evolutionary descendants of these BCGs from the present data, we can remark that the relatively large dynamical and H I masses measured for about two-thirds of our sample will function to inhibit the ejection of the ISM and to fuel future star formation. Although the current bursts of star formation are strong, they are unlikely to be the last nor could they produce the dominant stellar population in many of these galaxies. The remaining one-third of our sample shows, however, gas depletion timescales short enough to suggest that they could cease star formation in the near future and thus could be good candidates to undergo subsequent passive evolution.

Future work on this topic is essential. Higher spatial resolution H I data will help us resolve any confusion regarding the interpretation of our single-dish observations. It will also allow us to probe the internal structure of these galaxies to better understand how the effects of interactions may be affecting our calculated masses. Observations of the molecular gas in these galaxies will help determine the total gas mass available for star formation in these galaxies. Finally, observations of a much larger sample that is more representative of the BCG class at intermediate redshift is necessary to better infer the properties of their distant counterparts. This is the only way to divine the gaseous properties of the intermediate-redshift BCGs until we are capable of observing them directly.

We wish to thank the staff at the Arecibo Observatory for all their assistance and hospitality during our observations there. They helped make the observing run both enjoyable and successful. Special thanks to Snezana Stanimirovic, our "friend" at Arecibo, who went above and beyond the call of duty in helping us prepare for observing, observing, and reducing the data. We thank P. G. Pérez-Gonzalez for providing B magnitudes and $B-r$ colors for our sample galaxies. We also thank John Salzer, Liese van Zee, and David Koo for their comments, which helped improve the manuscript. The Digitized Sky Surveys were produced at the Space Telescope Science Institute under US government grant NAG W-2166. The images of these surveys are based on photographic data obtained using the Oschin Schmidt Telescope on Palomar Mountain and the UK Schmidt Telescope. The Second Palomar Observatory Sky Survey (POSS-II) was made by the California Institute of Tech-

nology with funds from the National Science Foundation, the National Geographic Society, the Sloan Foundation, the Samuel Oschin Foundation, and the Eastman Kodak Corporation. D. J. P. acknowledges partial support from the Wisconsin Space Grant Consortium. H. A. K. is grateful for support from Hubble Fellowship HF-01094.01-97A, awarded by the Space Telescope Science Institute. R. G.

acknowledges support from Hubble Fellowship HF-01092.01-97A, awarded by the Space Telescope Science Institute. J. G. acknowledges partial support from the Spanish Programa Sectorial de Promoción del Conocimiento under grant PB 96-0645. M. A. B. acknowledges support from NSF grant AST 99-70780 and LTSA contract NAG 5-6032.

REFERENCES

- Aaronson, M., Huchra, J., & Mould, J. 1980, *ApJ*, 237, 655
 Alonso-Herrero, A., Aragón-Salamanca, A., Zamorano, J., & Rego, M. 1996, *MNRAS*, 278, 417
 Barton, E. J., & van Zee, L. 2001, *ApJ*, 550, L35
 Bendo, G. J., & Barnes, J. E. 2000, *MNRAS*, 316, 315
 Bershad, M. A. 1997, in *ASP Conf. Ser. 117, Dark and Visible Matter in Galaxies*, ed. M. Persic & P. Salucci (San Francisco: ASP), 547
 Bershad, M. A., & Andersen, D. A. 2001, in *ASP Conf. Ser. 230, Galaxy Disks and Disk Galaxies*, ed. J. G. Funes, S. J. and E. M. Corsini (San Francisco: ASP), 589
 Bershad, M. A., Haynes, M. P., Giovanelli, R., & Andersen, D. R. 1999, in *ASP Conf. Ser. 182, Galaxy Dynamics*, ed. D. R. Merritt, M. Valluri, & J. A. Sellwood (San Francisco: ASP), 499
 Bershad, M. A., Jangren, A., & Conselice, C. J. 2000, *AJ*, 119, 2645
 Broeils, A. H. 1992, Ph.D. thesis, Univ. Groningen
 Conselice, C. J., Bershad, M. A., & Gallagher, J. S., III. 2000a, *A&A*, 354, L21
 Conselice, C. J., Bershad, M. A., & Jangren, A. 2000b, *ApJ*, 529, 886
 Courteau, S. 1997, *AJ*, 114, 2402
 de Vaucouleurs, G., de Vaucouleurs, A., Corwin, J. R., Buta, R. J., Paturel, G., & Fouqué, P. 1991, *Third Reference Catalogue of Bright Galaxies* (New York: Springer)
 Ellis, R. S. 1997, *ARA&A*, 35, 389
 Frei, Z. 1999, *Ap&SS*, 269, 649
 Forbes, D. A., Phillips, A. C., Koo, D. C., & Illingworth, G. D. 1996, *ApJ*, 462, 89
 Fukugita, M., Shimasaku, K., & Ichikawa, T. 1995, *PASP*, 107, 945
 Gallego, J., et al. 2001, in preparation
 Gallego, J., Zamorano, J., Rego, M., Alonso, O., & Vitores, A. G. 1996, *A&AS*, 120, 323
 Gallego, J., Zamorano, J., Rego, M., & Vitores, A. G. 1997, *ApJ*, 475, 502
 Guzmán, R., Gallego, J., Phillips, A., Koo, D., Lowenthal, J. D., Faber, S. M., Illingworth, G., & Vogt, N. 1997, *ApJ*, 489, 559
 Guzmán, R., Jangren, A., Koo, D. C., Bershad, M. A., & Simard, L. 1998, *ApJ*, 495, L13
 Guzmán, R., Koo, D. C., Faber, S. M., Illingworth, G. D., Takamiya, M., Kron, R. G., & Bershad, M. A. 1996, *ApJ*, 460, L5
 Hammer, F., Thuan, T. X., Cayatte, V., Guideroni, B., & Tran Van, T. H. 2000, in *Building Galaxies: From the Primordial Universe to the Present*, ed. F. Hammer, T. X. Thuan, V. Cayatte, B. Guideroni, & T. H. Tran Van (Singapore: World Sci.)
 Hernquist, L., & Mihos, J. C. 1995, *ApJ*, 448, 41
 Homeier, N. L., & Gallagher, J. S. 1999, *ApJ*, 522, 199
 Horellou, C., & Booth, R. 1997, *A&AS*, 126, 3
 Jangren, A., Bershad, M. A., Conselice, C. J., Koo, D. C., & Guzmán, R. 2001, *ApJ*, submitted
 Kennicutt, R. C. 1983, *ApJ*, 272, 54
 Kennicutt, R. C., Tamblyn, P., & Congdon, C. E. 1994, *ApJ*, 435, 22 (KTC)
 Kobulnicky, H. A., & Gebhardt, K. 2000, *AJ*, 119, 1608
 Koo, D. C., Bershad, M. A., Wirth, G. D., Stanford, S. A., & Majewski, S. R. 1994, *ApJ*, 427, L9
 Koo, D. C., Guzmán, R., Faber, S. M., Illingworth, G. D., Bershad, M. A., Kron, R. G., & Takamiya, M. 1995, *ApJ*, 440, L49
 Lehnert, M. D., & Heckman, T. M. 1996, *ApJ*, 462, 651
 Lowenthal, J. D., et al. 1997, *ApJ*, 481, 673
 Mallén-Ornelas, G., Lilly, S. J., Crampton, D., & Schade, D. 1999, *ApJ*, 518, L83
 Mathewson, D. S., Ford, V. L., & Buchhorn, M. 1992, *ApJS*, 81, 413
 Nordgren, T. E., Chengalur, J. N., Salpeter, E. E., & Terzian, Y. 1997a, *AJ*, 114, 77
 ———. 1997b, *AJ*, 114, 913
 Pérez-González, P. G., Zamorano, J., Gallego, J., & Gil de Paz, A. 2000, *A&AS*, 141, 409
 Pettini, M., Shapley, A. E., Steidel, C. C., Cuby, J.-G., Dickinson, M., Moorwood, A. F. M., Adelberger, K. L., & Giavalisco, M. 2001, *ApJ*, 554, 981
 Phillips, A. C., Guzmán, R., Gallego, J., Koo, D. C., Lowenthal, J. D., Vogt, N. P., Faber, S. M., & Illingworth, G. D. 1997, *ApJ*, 489, 543
 Pierce, M. J., & Tully, R. B. 1988, *ApJ*, 330, 579
 Raychaudhury, S., von Braun, K., Bernstein, G., & Guhathakurta, P. 1997, *AJ*, 113, 2046
 Rix, H.-W., Guhathakurta, P., Colless, M., & Ing, K. 1997, *MNRAS*, 285, 779
 Roberts, M. S., & Haynes, M. P. 1994, *ARA&A*, 32, 115
 Sanders, D. B., & Mirabel I. F. 1996, *ARA&A*, 34, 749
 Schade, D., Lilly, S. J., Crampton, D., Hammer, F., Le Fevre, O., & Tresse, L. 1995, *ApJ*, 451, L1
 Simard, L., & Pritchet, C. J. 1998, *ApJ*, 505, 96
 Smoker, J. V., Davies, R. D., Axon, D. J., & Hummel, E. 2000, *A&A*, 361, 19
 Steidel, C. C., Giavalisco, M., Dickinson, M., & Adelberger, K. L. 1996a, *AJ*, 112, 352
 Steidel, C. C., Giavalisco, M., Pettini, M., Dickinson, M., & Adelberger, K. L. 1996b, *ApJ*, 462, L17
 Taylor, C. L., Brinks, E., Grashuis, R. M., & Skillman, E. D. 1995, *ApJS*, 99, 427
 Telles, E., & Terlevich, R. 1993, *Ap&SS*, 205, 49
 Tully, R. B., & Fisher, J. R. 1977, *A&A*, 54, 661
 Tully, R. B., & Fouqué, P. 1985, *ApJS*, 58, 67
 van Zee, L., Skillman, E. D., & Salzer, J. J. 1998, *AJ*, 116, 1186
 Vitores, A. G., Zamorano, J., Rego, M., Alonso, O., & Gallego, J. 1996a, *A&AS*, 118, 7
 Vitores, A. G., Zamorano, J., Rego, M., Gallego, J., & Alonso, O. 1996b, *A&AS*, 120, 385
 Vogt, S. S., et al. 1994, *Proc. SPIE*, 2198, 362
 Vogt, N. P., Forbes, D. A., Phillips, A. C., Gronwall, C., Faber, S. M., Illingworth, G. D., & Koo, D. C. 1996, *ApJ*, 465, L15
 Vogt, N. P., et al. 1997, *ApJ*, 479, L121
 Young, L. M. 2000, *AJ*, 119, 188
 Young, L. M., & Lo, K. Y. 1997, *ApJ*, 490, 710
 Zamorano, J., Gallego, J., Rego, M., Vitores, A. G., & Alonso, O. 1996, *ApJS*, 105, 343
 Zamorano, J., Rego, M., Gallego, J., Vitores, A. G., González-Riestra, R., & Rodríguez-Caderot, G. 1994, *ApJS*, 95, 387